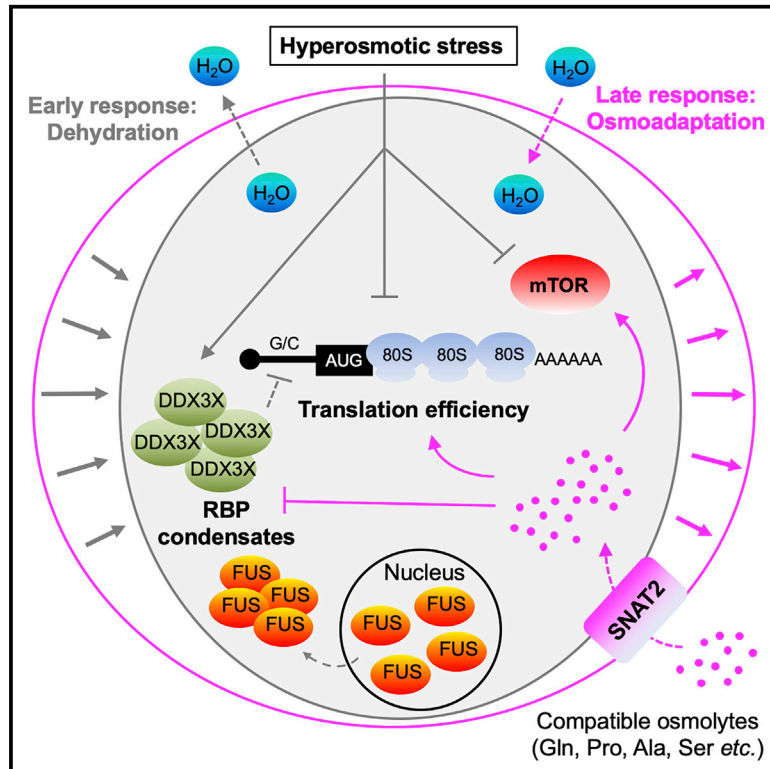# Stress-induced perturbations in intracellular amino acids reprogram mRNA translation in osmoadaptation independently of the ISR

Graphical abstract

Highlights

- SNAT2 activity mediates biphasic translational control in osmoadaptation

- Early-phase stress inhibits translation and induces distinct RBP condensates

- Late-phase SNAT2-mediated uptake of amino acids reverses translation inhibition

- SNAT2 activity disassembles early-phase RBP condensates

Authors

Dawid Krokowski, Raul Jobava,
Krzysztof J. Szkop, ..., Ivan Topisirovic,
Ola Larsson, Maria Hatzoglou

Correspondence

krokud@gmail.com (D.K.),
ivan.topisirovic@mcgill.ca (I.T.),
ola.larsson@ki.se (O.L.),
mxh8@case.edu (M.H.)

In brief

Krokowski et al. report that osmotolerance, in response to mild hypertonic stress, involves a biphasic response of translational control that includes the amino acid transporter SNAT2 and mTOR, independently of ISR. SNAT2-mediated amino acid uptake functions as a critical molecular switch of the biphasic response and thus establishment of osmoadaptation.

Cell Reports

Article

Stress-induced perturbations in intracellular amino acids reprogram mRNA translation in osmoadaptation independently of the ISR

Dawid Krokowski,[1,2,13,*] Raul Jobava,[1,3,13] Krzysztof J. Szkop,[4,13] Chien-Wen Chen,[1] Xu Fu,[5] Sarah Venus,[3] Bo-Jhih Guan,[1] Jing Wu,[1] Zhaofeng Gao,[1] Wioleta Banaszuk,[2] Marek Tchorzewski,[2,6] Tingwei Mu,[5] Phil Ropelewski,[5] William C. Merrick,[3] Yuanhui Mao,[7] Aksoylu Inci Sevval,[4] Helen Miranda,[1] Shu-Bing Qian,[7] Maria Manifava,[8] Nicholas T. Ktistakis,[8] Anastasios Vourekas,[9] Eckhard Jankowsky,[3] Ivan Topisirovic,[10,11,12,*] Ola Larsson,[4,*] and Maria Hatzoglou[1,14,*]

[1]Department of Genetics and Genome Sciences, School of Medicine, Case Western Reserve University, Cleveland, OH, USA
[2]Department of Molecular Biology, Institute of Biological Sciences, Maria Curie-Skłodowska University, Lublin, Poland
[3]Department of Biochemistry, School of Medicine, Case Western Reserve University, Cleveland, OH, USA
[4]Department of Oncology-Pathology, Science for Life Laboratories, Karolinska Institute, Stockholm, Sweden
[5]Department of Physiology and Biophysics, School of Medicine, Case Western Reserve University, Cleveland, OH, USA
[6]EcoTech-Complex Centre, Maria Curie-Skłodowska University, Lublin, Poland
[7]Division of Nutritional Sciences, Cornell University, Ithaca, NY 14853, USA
[8]Signalling Programme, Babraham Institute, Cambridge, UK
[9]Department of Biological Sciences, Louisiana State University, Baton Rouge, LA 70803, USA
[10]The Lady Davis Institute, Jewish General Hospital, Montréal, QC, Canada
[11]Gerald Bronfman Department of Oncology, McGill University, Montréal, QC, Canada
[12]Department of Biochemistry and Division of Experimental Medicine, McGill University, Montréal, QC, Canada
[13]These authors contributed equally
[14]Lead contact
*Correspondence: krokud@gmail.com (D.K.), ivan.topisirovic@mcgill.ca (I.T.), ola.larsson@ki.se (O.L.), mxh8@case.edu (M.H.)
https://doi.org/10.1016/j.celrep.2022.111092

SUMMARY

The integrated stress response (ISR) plays a pivotal role in adaptation of translation machinery to cellular stress. Here, we demonstrate an ISR-independent osmoadaptation mechanism involving reprogramming of translation via coordinated but independent actions of mTOR and plasma membrane amino acid transporter SNAT2. This biphasic response entails reduced global protein synthesis and mTOR signaling followed by translation of SNAT2. Induction of SNAT2 leads to accumulation of amino acids and reactivation of mTOR and global protein synthesis, paralleled by partial reversal of the early-phase, stress-induced translatome. We propose SNAT2 functions as a molecular switch between inhibition of protein synthesis and establishment of an osmoadaptive translation program involving the formation of cytoplasmic condensates of SNAT2-regulated RNA-binding proteins DDX3X and FUS. In summary, we define key roles of SNAT2 in osmotolerance.

INTRODUCTION

Adaptation to increased extracellular osmolarity requires accumulation of osmolytes in the cytoplasm to restore cell volume (Hoffmann et al., 2009). Activation of plasma membrane channels leads to an increase of ions in the cytoplasm (Eveloff and Warnock, 1987; Pedersen et al., 2007), later replaced with organic osmolytes such as amino acids. This accumulation of compatible osmolytes results from a combination of increased biosynthesis and extracellular uptake (Burg et al., 1997; Bussolati et al., 2001). The second phase of the response involves transcription of genes encoding membrane transporters and factors involved in metabolic reprogramming (Burg et al., 1997; Franchi-Gazzola et al., 2004). Several models show that transcription of the gene encoding amino acid transporter SNAT2 (SLC38A2) increases upon increased osmolarity (Bussolati et al., 2001; Fran-chi-Gazzola et al., 1999, 2006; Krokowski et al., 2015). SNAT2 is a sodium-dependent transporter of small neutral amino acids Gly, Ala, Pro, Ser, and Gln (Broer, 2014). Loss of SNAT2 activity decreases cell viability in hyperosmotic conditions, confirming its importance in osmoadaptation (Bevilacqua et al., 2005; Krokowski et al., 2017).

In addition to osmotic stress, conditions that induce the integrated stress response (ISR) also induce transcription of SLC38A2. The ISR is a cytoprotective response to diverse stressors initiated by phosphorylation of the α subunit of eukaryotic translation initiation factor 2 (eIF2α-P) (Costa-Mattioli and Walter, 2020). Phosphorylated eIF2α binds to eIF2B, thereby decreasing its guanine nucleotide exchange factor (GEF) activity (Costa-Mattioli and Walter, 2020), resulting in decreased translation initiation (Baird and Wek, 2012). Upon induction of the ISR, translation of mRNAs harboring upstream open reading frames,

such as *ATF4*, is upregulated (Hinnebusch et al., 2016), leading to an increase in *SLC38A2* transcription (Guan et al., 2014; Han et al., 2013; Krokowski et al., 2013). Consequently, amino acid content increases upon ATF4 induction (Guan et al., 2014; Krokowski et al., 2013).

Even though high-intensity hyperosmotic stress induces eIF2α phosphorylation, translation of *ATF4* mRNA and ATF4 protein levels remain unaltered (Jobava et al., 2021; Krokowski et al., 2015). Instead, induction of SNAT2 is mediated by transcription factors tonicity enhancer binding protein TonEBP and the nuclear factor κB (NF-κB) family protein c-Rel (Farabaugh et al., 2020; Maallem et al., 2008). In contrast to the ISR, mild hyperosmotic-stress-associated SNAT2 induction is not accompanied by global upregulation of amino acid transporters (Burg et al., 2007; Maallem et al., 2008).

Alterations in SNAT2 activity are paralleled by changes in mTOR signaling; overexpression of SNAT2 in hepatocytes leads to hyperactivation of the mTOR pathway (Uno et al., 2015), while SNAT2 inhibition leads to decreased mTOR activity and reduced proliferation (Pinilla et al., 2011). Among SNAT2 substrates, the link between Gln and mTOR activation is best understood (Broer, 2014). While SNAT2 minimally contributes to Gln uptake under baseline conditions, it acts as a "responder" to different stress conditions (Broer et al., 2016). Two mechanisms contribute to increased mTOR kinase activity after SNAT2 induction: (1) the transporter LAT1 (SLC7A5) exports Gln, supporting uptake of branch-chain amino acids (BCAAs) that are potent mTOR inducers (Nicklin et al., 2009), and (2) mTOR activity can be directly stimulated by increased intracellular Gln (Jewell et al., 2015).

As dry eye syndrome is a result of corneal epithelial cell exposure to mild hyperosmotic stress, we employed these cells to study the mechanisms of osmoadaptation. Our results reveal a biphasic response to hyperosmotic stress; the early phase is characterized by reduction in protein synthesis and suppressed mTOR activity, followed by a SNAT2-mediated osmoadaptive phase characterized by translation reprogramming and partial recovery of translation and mTOR activity. Strikingly, the mechanism underlying SNAT2-mediated translation reprogramming in osmoadaptation is distinct from that induced by eIF2α-P and the ISR. We provide evidence that SNAT2-mediated amino acid uptake promotes osmoadaptive recovery of protein synthesis by selectively reversing stress-repressed translation while sustaining mTOR activity (Masvidal et al., 2017). This biphasic response is also accompanied by an increase of cytoplasmic condensates of RNA-binding proteins (RBPs), reversed by SNAT2 activity during the transition to osmoadaptation.

RESULTS

Regulation of protein synthesis in corneal epithelial cells exposed to hyperosmotic stress

To investigate the recovery of protein synthesis during osmoadaptation, we exposed human corneal epithelial cells to mild (500 mOsm) or severe (600 mOsm) osmotic stress. While severe stress suppressed protein synthesis with no recovery (Krokowski et al., 2017), protein synthesis recovered substantially after mild stress (Figures 1A and 1B). We found both mild and severe hyperosmotic stress significantly decreased mTOR activity, evi-

denced by a reduction in phosphorylation of p70S6K (Figure 1C). In contrast, phosphorylation of eIF2α was increased only by severe stress. These effects were independent of the nature of the osmolyte used (NaCl or sorbitol). Although mild stress did not induce eIF2α phosphorylation, it dramatically reduced protein synthesis, suggesting that in corneal epithelial cells, regulation of protein synthesis under mild hyperosmotic stress may be independent of eIF2α phosphorylation.

To further assess the contribution of eIF2α signaling to protein synthesis recovery, we measured GEF activity of eIF2B (Guan et al., 2017; Kimball et al., 1989). Consistent with lack of change in eIF2α phosphorylation, we did not observe changes in GEF activity in mild stress (Figure 1D). We confirmed these findings using ISRIB, which induces eIF2B dimerization leading to a decrease in eIF2B sequestration by phosphorylated eIF2α (Tsai et al., 2018; Zyryanova et al., 2018). We have previously shown that ISRIB can inhibit the ISR in human corneal epithelial cells exposed to endoplasmic reticulum (ER) stress (Krokowski et al., 2017). Consistent with a lack of ISR activation, ISRIB did not affect global protein synthesis rates in mild stress (Figure 1E). Due to the apparent lack of ISR during adaptation to mild osmotic stress, we investigated the role of the mTOR pathway. We observed that mTOR activity, as determined by p70S6K and 4E-BP1 phosphorylation (Figure 1F), mirrored adaptive protein synthesis recovery. Indeed, the presence of mTOR inhibitor torin 1 (Figures 1G, 100 nM, and 1H, 10 nM) during the last hour of treatment dramatically attenuated protein synthesis recovery as measured by puromycylation or ^{35}S-Met/Cys labeling. Collectively, these data suggest that mTOR, but not the ISR, is a major regulator of osmoadaptive protein synthesis.

SNAT2 reshapes intracellular amino acid composition during osmoadaptation

Adaptation to increased osmolarity involves SNAT2 induction and delivery to the plasma membrane (Krokowski et al., 2017). The window of osmoadaptation was between 400 and 560 mOsm (Figure 1I). Consistently, we observed increased uptake of SNAT2 substrate Pro in corneal epithelial cells under mild hyperosmotic stress (Figure S1A), and the addition of MeAIB, a non-metabolized SNAT2 substrate, abolished these effects, demonstrating that the increase in Pro uptake is SNAT2 dependent. Furthermore, Gln uptake decreases upon hyperosmotic stress, reaching 80% of the basal level after 3 h (Figure S1B). This is paralleled by decreased expression of mRNA encoding Gln transporter ASCT2 (SLC1A5) (Figure S1C). However, the reduction in *ASCT2* mRNA could not explain the recovery of Gln uptake from 3 to 6 h of treatment (Figure S1B). Because increased Gln uptake correlates with induction of SNAT2 activity, we tested whether MeAIB interferes with Gln uptake. We found that MeAIB reduced Gln uptake over the course of hyperosmotic stress (Figure 2A), suggesting that SNAT2 contributes to Gln uptake during mild stress. To further corroborate this, we examined the impact of Thr on Gln transport, as Thr is an optimal substrate for ASCT2 and SLC6A14 but has weak affinity for SNAT2 (Broer, 2014; Kanai et al., 1992; Karunakaran et al., 2011). Thr inhibited the uptake of Gln in unstressed cells, but this was attenuated in mild stress (Figure S1D), further supporting the contribution of SNAT2 to Gln uptake during osmoadaptation. LAT1 plays a
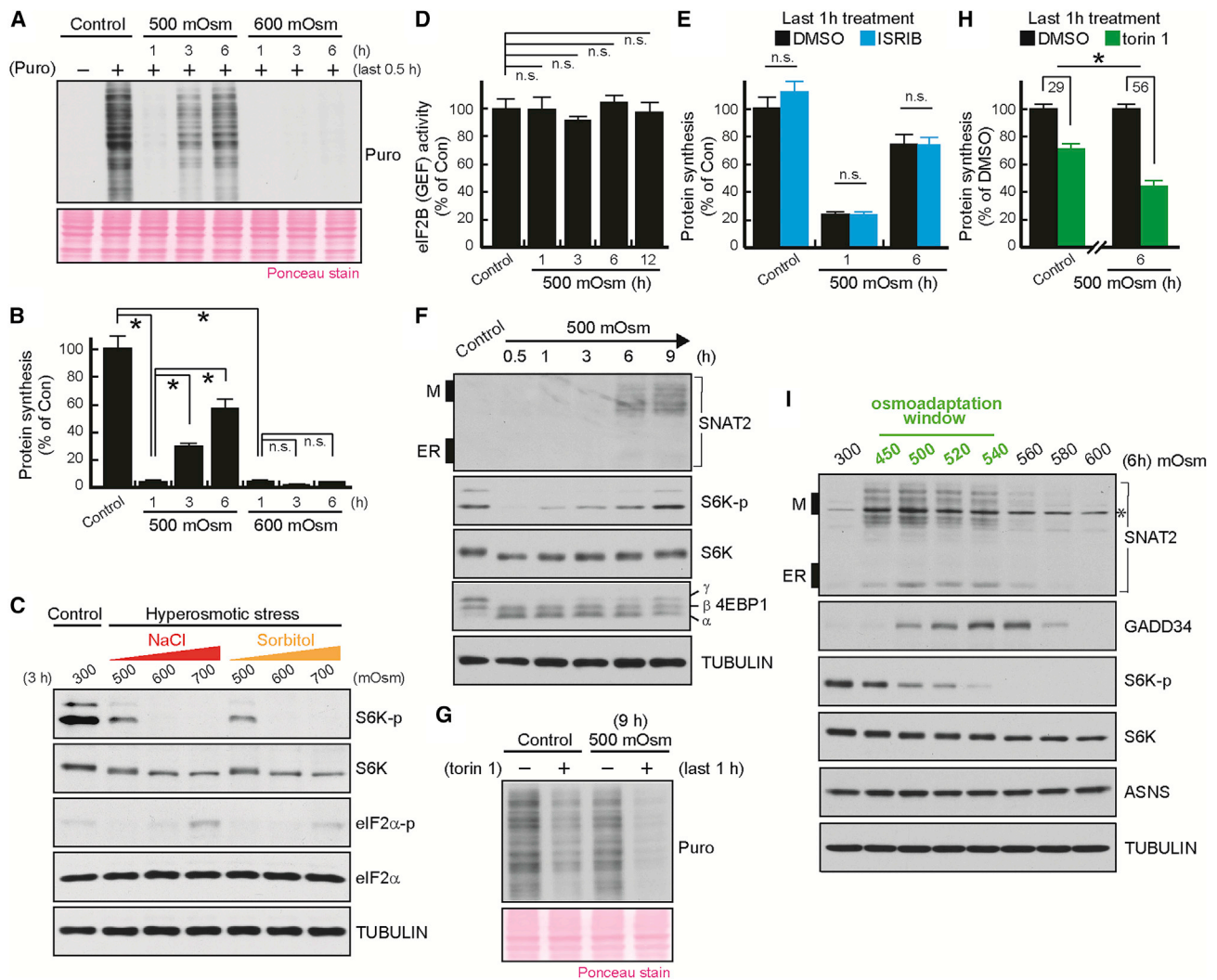
Figure 1. Regulation of protein synthesis in corneal epithelial cells exposed to mild hyperosmotic stress involves mTOR but not eIF2α phosphorylation

(A) Protein synthesis rates in cells challenged with 500 and 600 mOsm media (NaCl) measured by puromycin incorporation.

(B) Densitometric quantification of (A), n = 3, error bars represent SEM,*p < 0.01; n.s., not significant.

(C) Western blot analysis of eIF2α and mTOR signaling pathways in cells challenged with sorbitol or NaCl.

(D) GEF activity of eIF2B in cells cultured in 500 mOsm media (NaCl).Error bars represent SEM, n.s., not significant.

(E) Protein synthesis rates as measured by incorporation of ^{35}S-labeled Cys/Met in cells exposed to 500 mOsm (NaCl) media in the presence of ISRIB (100 nM) during the last 1 h of treatment, n = 4, error bars represent SEM, *p < 0.01; n.s., not significant.

(F and I) Western blot analysis of cells challenged with NaCl. M, mature plasma membrane SNAT2 protein; ER, endoplasmic reticulum intermediate in the maturation process of SNAT2 protein. Asterisk indicates a non-specific protein band.

(G) Impact of the mTOR inhibitor torin 1 (100 nM, last 1 h of treatment) on puromycin incorporation during 500 mOsm hyperosmotic stress (NaCl).

(H) Protein synthesis measured by ^{35}S-labeled Cys/Met labeling in the presence of mTOR inhibitor torin 1 (10 nM, last 1 h of treatment) with 500 mOsm media (NaCl). Data are normalized to percentage of incorporation in cells without torin 1 treatment, n = 4, error bars represent SEM, *p < 0.01.

central role in the uptake of extracellular BCAAs, including Leu (Nicklin et al., 2009), in exchange for intracellular Gln. We found a gradual increase in Leu uptake, indicative of upregulated LAT1 activity, during mild hyperosmotic stress (Figure 2B). The observed increase in LAT1 activity paralleled increased SNAT2 activity (Figures 2B and S1A). Blocking SNAT2 activity during the last hour of mild hyperosmotic treatment attenuated Leu uptake (Figure 2B), suggesting that increased activity of SNAT2

may mediate Leu uptake during adaptation to hyperosmotic stress by providing Gln as an efflux substrate for LAT1 (Figure 2C).

To investigate the involvement of SNAT2 in amino acid homeostasis, we depleted SNAT2 using short hairpin RNA (shRNA) (Figures S1E–S1G). These cells showed no significant difference in basal Pro uptake, while having abrogated hyperosmotic stress-induced SNAT2 activity (Figure 2D), in agreement with
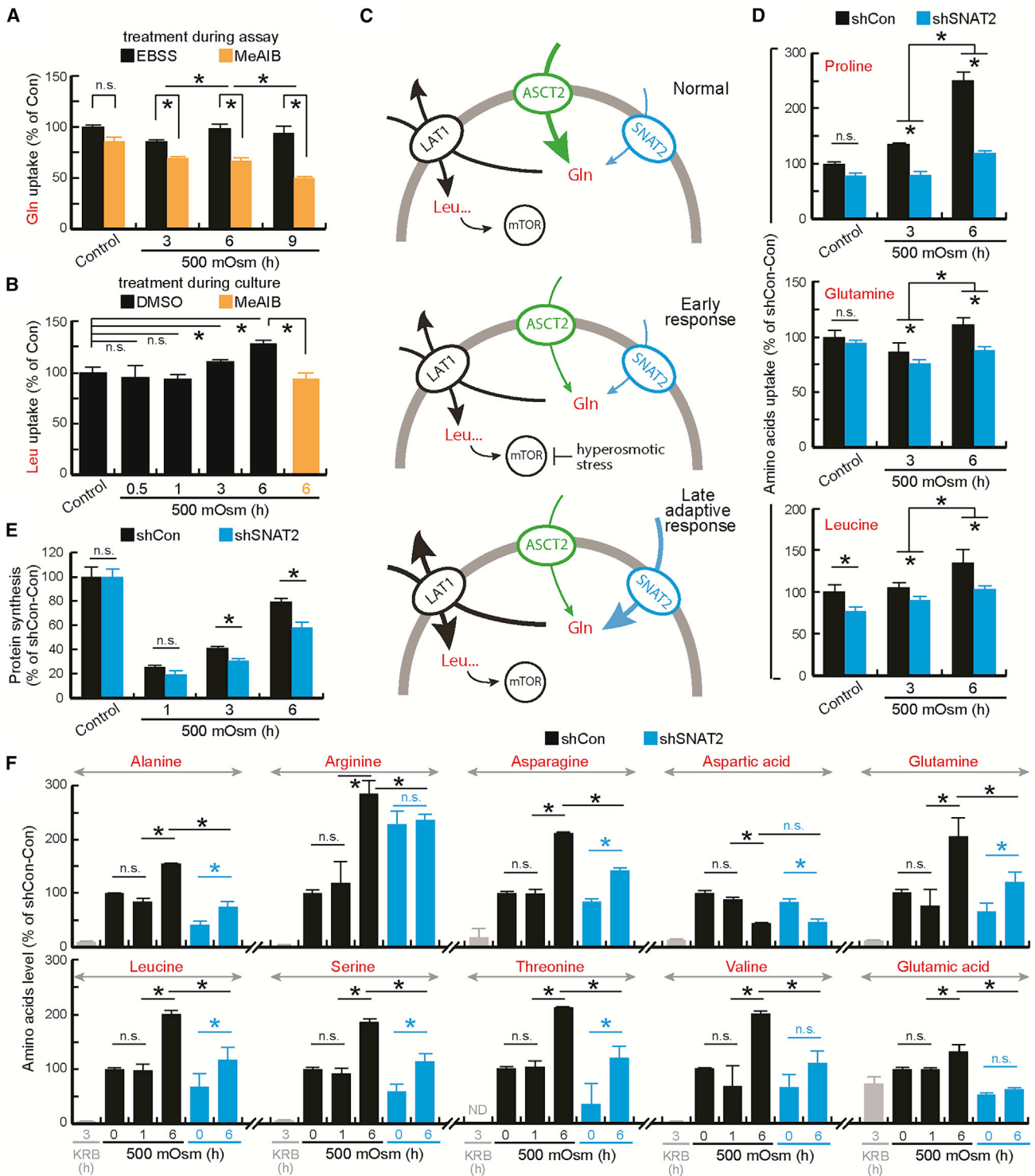
Figure 2. Contribution of SNAT2 to changes in amino acid uptake during hyperosmotic stress in human corneal epithelial cells

(A–F) NaCl was used to increase osmolarity.

(A) Gln uptake during hyperosmotic treatment (500 mOsm) in the presence or absence of MeAIB (5 mM). Error bars represent SEM, p < 0.01; n.s., not significant.

(B) Leu uptake for the indicated treatments. MeAIB (5 mM) was added to the media for the last 1 h of treatment. Error bars represent SEM, p < 0.01; n.s., not significant.

(C) Schematic representation of the regulation of Gln transporters in the adaptive recovery of mTOR activity. In normal osmolarity, uptake of Gln by ASCT2 provides an efflux substrate for Leu uptake by LAT1. Leu activates mTOR via an amino acid sensing mechanism and promotes protein synthesis. In the early

(legend continued on next page)

the decreased Gln uptake upon hyperosmotic challenge. Furthermore, downregulation of Gln uptake was accompanied by decreased Leu uptake (Figure 2D), attenuated protein synthesis recovery (Figure 2E), and reduced re-activation of mTOR (Figures S1F–S1G).

To directly determine the contribution of SNAT2 to amino acid homeostasis, we assessed free amino acid content in corneal epithelial cells. We tested the system by exposing corneal epithelial cells to an amino-acid-free media (Krebs-Ringer modified buffer [KRB]). As expected, KRB treatment dramatically decreased levels of intracellular amino acids, with the exception of Glu (Figure 2F). Next, we assessed the effects of hyperosmotic complete media on intracellular amino acid concentrations. While one hour of hyperosmotic stress did not change amino acid content, prolonged exposure increased levels of SNAT2 substrates Ala and Gln (Figure 2F). Because any single amino acid can be a substrate for more than one obligatory exchanger, its accumulation can lead to the uptake of a variety of amino acids, explaining how increased intracellular Gln drives uptake of other amino acids, including Leu, Thr, Ser, and Val (Figure 2F). Interestingly, levels of Asn increased while levels of Asp decreased, without changes of ASNS levels (Figures S1H and S1I). Absence of amino acid starvation-induced ISR during osmoadaptation (Al-Baghdadi et al., 2017) was also confirmed with pharmacological inhibition of the GCN2 kinase (Figure S1I). Cells expressing shRNA against SNAT2 under control conditions had decreased levels of Ala and Gln that were mirrored by decreases in Leu, Thr, Ser, and Val (Figure 2F). Moreover, during stress, increases in levels of SNAT2 substrates and other amino acids were abolished in cells with reduced SNAT2 expression (Figure 2F). Intriguingly, under non-stressed conditions, the levels of Arg in cells with compromised SNAT2 expression were higher than in controls, suggesting that SNAT2 may also act as part of the amino acid transporter network under basal conditions. In summary, these data suggest that SNAT2 plays a major role in regulation of intracellular amino acid content during osmoadaptation.

Stress-induced perturbations in protein synthesis are independent of eIF2α phosphorylation

To further investigate the role of eIF2α phosphorylation during protein synthesis recovery, we used mouse embryonic fibroblasts (MEFs) expressing non-phosphorylatable eIF2α (S51A), which are ISR deficient (Scheuner et al., 2001). We previously showed that S51A MEFs induce expression of SNAT2 in response to mild hyperosmotic stress (Krokowski et al., 2017).

Similar to corneal epithelial cells, S51A MEFs treated with sorbitol showed a biphasic response wherein early inhibition of protein synthesis was followed by recovery (Figure S2A), which was correlated with SNAT2 induction and mTOR re-activation (Figure S2B). Similar to depletion in corneal epithelial cells, CRISPR-mediated abrogation of SNAT2 (SNAT2 knockout [KO]) abolished recovery of mTOR activity in S51A MEFs (Figure S2B). Because MEFs do not require growth factors in addition to serum, we asked whether growth factors were required for mTOR modulation during osmoadaptation. As expected, serum withdrawal led to suppressed mTOR signaling in S51A MEFs (Figure S2C). Strikingly, even in serum-deprived conditions, mTOR activity was dynamically regulated in response to sorbitol-induced hyperosmotic stress and was still dependent on SNAT2 (Figure S2C). Moreover, SNAT2 inhibition or sdepletion of Gln also attenuated mTOR reactivation in serum-free media (Figure S2D), suggesting that regulation of mTOR during osmoadaptive stress in MEFs is growth factor-independent.

We previously demonstrated that induction of the PP1 phosphatase subunit GADD34 by hyperosmotic stress is necessary for posttranslational processing and efficient plasma membrane localization of SNAT2 (Krokowski et al., 2017). Here, we found that GADD34 is induced during the window of osmoadaptation in cells exposed to hyperosmotic stress (Figure 1I). The function of GADD34/PP1 in protein trafficking during hyperosmotic stress is independent of its functions in the ISR (Novoa et al., 2001). We found that GADD34/PP1 inhibitors sephin1 and the salubrinal derivative Sal003 decreased accumulation of mature SNAT2 and attenuated mTOR reactivation during stress in S51A MEFs (Figure S2D). Similar to corneal epithelial cells (Figure S1A), we found that in MEFs' mild hyperosmotic stress increased SNAT2 activity (Figure S2E) and Gln uptake (Figure S2F). Therefore, modulation of mTOR activity during osmoadaptation is amino-acid- and SNAT2 dependent, growth factor- and eIF2α-P independent, and requires GADD34/PP1 activity.

Osmoadaptive recovery of mTOR activity involves Leu-sensing

To further investigate the role of SNAT2 in reactivating mTOR during osmoadaptation, we used di-leucine methyl ester (LLME), which stimulates mTOR in absence of amino acids (Manifava et al., 2016). Uptake of LLME is independent of amino acid transporters, and it is hydrolyzed in the lysosomes to increase the lysosomal Leu pool (Ransom and Reeves, 1983). Consequently, LLME treatment recruits mTOR to the lysosomal membrane via a Leu-sensing mechanism (Manifava et al., 2016;

response to increased osmolarity, the activity and levels of ASCT2 decrease and the amino acid sensing mechanism that activates mTOR is attenuated, inhibiting mTOR and protein synthesis. In the late osmoadaptive phase, the amino acid sensing mechanism, mTOR activity, and inhibition of protein synthesis are restored via increased levels of SNAT2.

(D) Pro, Gln, and Leu uptake during adaptation to increased osmolarity (500 mOsm) in cells expressing shCon or shRNA (#2) against SNAT2. Error bars represent SEM, p < 0.01; n.s., not significant.

(E) Control (shCon) or cells expressing shRNA (#2) against SNAT2 were exposed to increased osmolarity (500 mOsm). Protein synthesis was measured by ^{35}S-labeled Cys/Met incorporation during adaptation to increased osmolarity.

In (A), (B), (D), and (E), n = 4–6, error bars represent SEM, *p < 0.01; n.s., not significant.

(F) Normalized levels of the indicated amino acids in control cells (shCon) or cells expressing shRNA against SNAT2 (#2) during adaptation to increased osmolarity (500 mOsm). Krebs-Ringer bicarbonate buffer (KRB) treatment for 3 h was used to induce amino acid deficiency as a control. n = 3, error bars represent SEM, *p < 0.01; n.s., not significant.

Sancak et al., 2010; FWolfson et al., 2016). We show that removal of amino acids from the media resulted in mTOR inactivation in S51A MEFs, and subsequent treatment with LLME partially restored mTOR activity (Figure S2G). Addition of Leu alone had no immediate impact on mTOR activity. At the time of maximum mTOR suppression, we show that addition of LLME, but not Leu, stimulated mTOR activity (Figure S2H). Strikingly, LLME had no impact on mTOR activity during osmoadaptation (Figure S2H). These findings further support a SNAT2-mediated mechanism of mTOR and protein synthesis recovery during osmoadaptation. Of note, LLME only partially reversed stress-associated inhibition of mTOR, suggesting that other mechanisms also contribute to hyperosmotic-stress-associated suppression of mTOR activity. In agreement with this, S51A MEFs treated with up to 700 mOsm media were insensitive to LLME-dependent re-activation of mTOR, which correlated with loss of osmoadaptive protein synthesis recovery (Figures S2I–S2J). Taken together, these data demonstrate that, in MEFs, hyperosmotic-stress-dependent regulation of mTOR involves Leu sensing.

Hyperosmotic stress induces selective translation of osmoadaptive mRNAs

Hyperosmotic stress and osmoadaptation are associated with dramatic modulation of global protein synthesis. Polysome tracings revealed a reduction and partial recovery of polysomes during early and late osmoadaptation phases, respectively (Figures 1A–1B and S3A). To assess whether the response to mild hyperosmotic stress was associated with transcript-selective alterations in mRNA translation, we captured translation landscapes in corneal epithelial cells after 1 and 6 h of mild hyperosmotic stress to mimic the early stress and osmoadaptation phases, respectively (Figure 3A). We employed ribosome profiling to analyze the distribution of ribosome footprints with sub-codon resolution (Ingolia et al., 2009). RNA libraries were generated from ribosome-protected fragments (RPFs) and total RNA from all conditions (Table S1). As expected, a majority of reads mapped to coding regions and showed a clear 3-nucleotide periodicity (Figure S4A). Moreover, by applying RUST (O'Connor et al., 2016) meta footprint profiles, we excluded potential biases from preparation of RPF libraries (Figure S4B). Importantly, the complexity of libraries from total mRNA and RPFs were comparable (Figure S4C), and the obtained sequencing depths met the threshold required for reliable analysis (Figure S4C; Table S1). We assessed dataset reproducibility using principal-component analysis (PCA), which indicated separation of samples based on source of RNA (i.e., total or RPF) and treatment (Figures S4D–S4E). Changes in gene expression between conditions were captured using anota2seq (Oertlin et al., 2019) (Table S1), which assesses three modes of regulation: (1) changes in RPFs congruent with changes in total mRNA levels ("mRNA abundance"), (2) alterations in RPFs not accompanied by corresponding changes in total mRNA levels ("translation"), and (3) changes in total mRNA levels not accompanied by corresponding changes in RPFs ("buffering"). After 1 h of 500 mOsm stress, translations of numerous mRNAs including those encoding SNAT2, GADD34, the taurine transporter SLC6A6, and TonEBP were increased (Figure 3B). The increase in *SLC38A2* mRNA translation observed from ribosome-profiling data was validated

by polysome profiling (Figures S3A–S3B). However, synthesis of osmoadaptive proteins was not unidirectional, as translation of mRNAs encoding the SLC12A2 Na+-K+-2Cl− cotransporter (Liedtke and Cole, 2002) or SLC9A3R2 scaffolding protein coordinating Na+/H+ exchange (Uawithya et al., 2008) were translationally suppressed (Figure 3B). In contrast to pervasive alterations in translation, changes in mRNA abundance and translation buffering were confined to a limited number of transcripts (Figure 3B). Therefore, early-phase hyperosmotic stress causes selective reprogramming of mRNA translation.

Adaptation to hyperosmotic stress involves reversal of early-phase alterations in translation

In addition to translation perturbations, the osmoadaptation phase also involved changes in mRNA abundance (408 upregulated and 481 downregulated mRNAs; Figure 3C). Strikingly, mRNAs whose levels were induced included those encoding SNAT2, GADD34, TonEBP, and SLC6A6 that were translationally activated during the early phase of the stress response (Figures 3B and 3C), consistent with previous reports (Ferraris and Burg, 2006). Moreover, mRNAs encoding SLC12A2 or SLC9A3R2, translationally suppressed during the early phase, were translationally activated during osmoadaptation (Figures 3B and 3C). These data suggest osmoadaptation involves two distinct phases: (1) an early phase of translational reprogramming to selective translation of mRNAs encoding a subset of regulators of osmoadaptation, and (2) a late phase signified by orchestrated induction of transcriptional and translation programs to sustain the osmoadaptive proteome.

To determine how these translation programs are orchestrated, we first determined how transcripts with altered translation during early stress were regulated during the adaptive phase. We found partial reversal of the early stress-induced translation program during the adaptive phase, as 60% of mRNAs showing increased translation during the early phase were translationally suppressed during osmoadaptation, and 74% of mRNAs translationally suppressed during the early phase exhibited increased translation during the late phase (Figure 3D). Indeed, remodeling of translation during the late phase was dominated by a reversal of early-phase effects (Figure S5A). In contrast, most transcripts whose abundance was altered during the late phase were not modulated during the early phase (Figure S5A). Finally, mRNAs translationally buffered during the osmoadaptive phase largely exhibited changes in translation anticipated to alter protein levels during the early phase. These ribosomal-profiling studies suggest that while osmoadaptive proteins are translationally activated during the early stress phase, their levels are further induced by coordinated changes in mRNA abundance during the late adaptive phase (Figures 3C, S3A, and S3B).

Of note, relative to unstressed cells, observed translation perturbations were mostly driven by the early phase, including 145 out of 178 translationally activated (81%) and 425 out of 601 translationally suppressed (70%) mRNAs (Figures 3E and 3F). A large subset of mRNAs whose translation was increased during early stress had higher abundance during the late adaptive phase (189 transcripts; Figure 3F), including the RNA helicases DDX5 and DDX3X, known to regulate mRNA translation (Calviello et al., 2021; Hoch-Kraft et al., 2018). Collectively, these data show the transition to osmoadaptation involves dramatic and
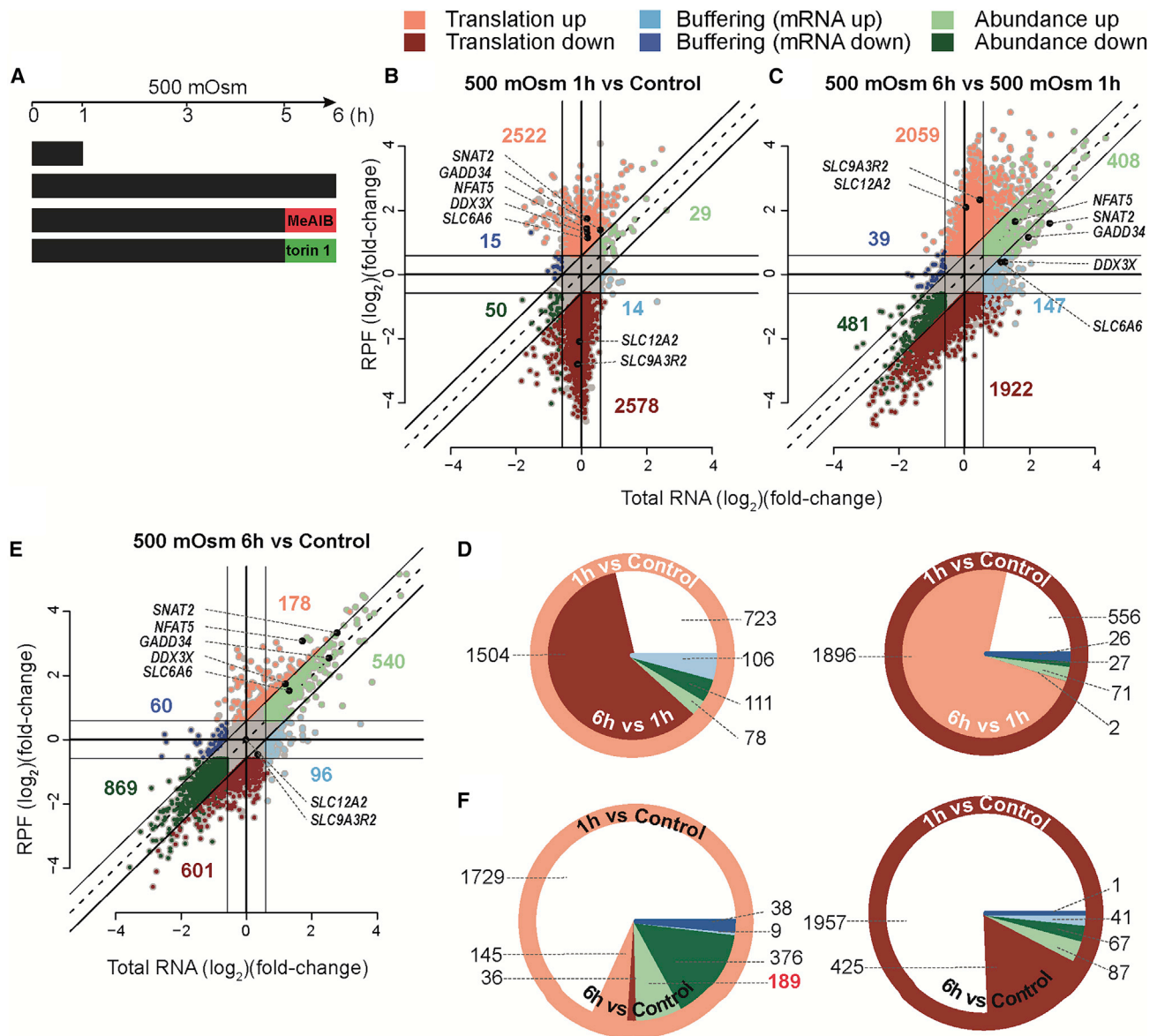
Figure 3. Changes in mRNA translation and abundance mark progression to osmoadaptation

(A) Schematic of conditions for ribosome profiling experiments.

(B and C) Scatterplots of RPF versus total mRNA fold changes (average across replicates) comparing the early (1 h 500 mOsm, NaCl versus control; B) and adaptive (6 h 500 mOsm versus 1 h 500 mOsm, NaCl; C) phases. The numbers of mRNAs show changes in translation (upregulated, light red, and downregulated, dark red), buffering, or abundance as determined by anota2seq. Select transcripts encoding osmoadaptive proteins are highlighted.

(D) Pie charts of the subset of transcripts identified under individual comparisons (indicated by the rim) and their regulation under a second comparison (indicated by pie slices). The top graph assesses how transcripts whose translation was activated (color of the rim) when comparing 1 h 500 mOsm stress with control (text in the rim) are regulated between 6 and 1 h 500 mOsm (text in the pie) of osmotic stress (color of pie slices indicate mode of regulation as in B and C; no regulation: white); the number of transcripts underlying the size of each pie slice are also indicated. The lower plot shows how transcripts whose translation was suppressed during the early mild-hyperosmotic-stress phase (1 h 500 mOsm) are regulated during the adaptation phase (6 h 500 mOsm).

(E) Similar to (B) and (C), comparing 6 h of the 500 mOsm (NaCl) hyperosmotic stress with control.

(F) Pie charts as in (D) comparing how transcripts translationally activated (left) or suppressed (right) during the early phase of mild hyperosmotic stress (1 h 500 mOsm) are regulated when comparing 6 h 500 mOsm with the control condition.
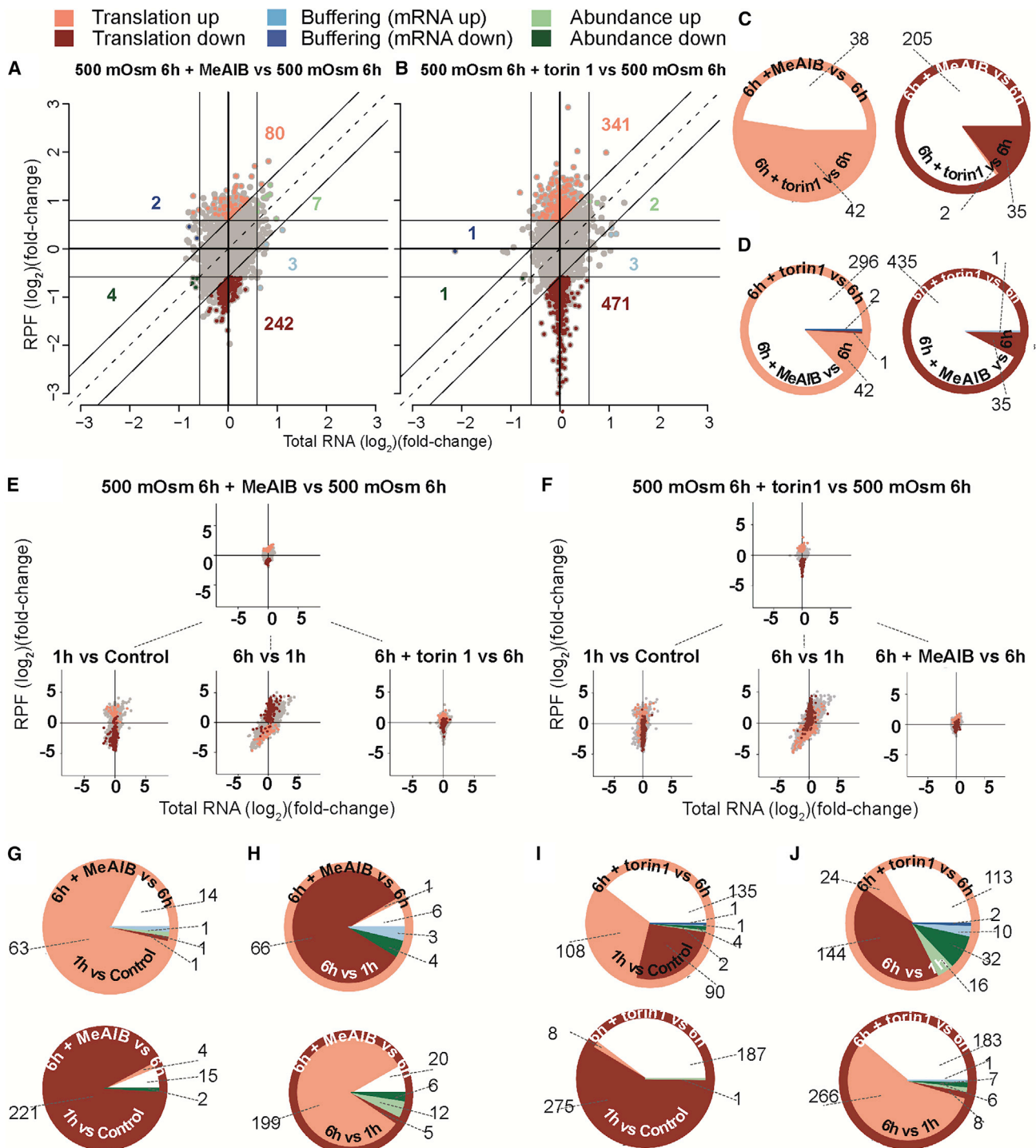
Figure 4. SNAT2 and mTOR independently affect translation during mild stress

(A and B) Scatterplots as described in Figures 3B and 3C comparing the effects of MeAIB (A) or torin 1 (B) treatments during the last 1 h of a 6 h 500 mOsm (NaCl) treatment to the same treatment in absence of inhibitors.

(C and D) Pie charts as described in Figure 3D comparing how transcripts whose translation was modulated by MeAIB were regulated by torin 1 (C) or how those mRNAs whose translation was affected by torin 1 were regulated by MeAIB (D).

(E) Scatterplots as described in Figures 3B and 3C assessing how transcripts identified in (A) are regulated under early (1 h 500 mOsm; bottom left) or adaptive (6 h 500 mOsm) mild hyperosmotic stress phases in the absence (bottom center) or presence (bottom right) of torin 1.

(legend continued on next page)

orchestrated changes in translation programs and mRNA abundance.

Regulation of chaperones during osmoadaptation

Hyperosmotic stress causes macromolecular crowding, which can lead to protein aggregation. Although protective in mild stress conditions, this causes irreversible cell damage during prolonged or severe stress (Santra et al., 2018). Cells employ chaperone proteins to counteract protein aggregation (Feleciano et al., 2019). We noted that 8 mRNAs encoding heat shock chaperones showed increased translation during the early phase of the mild hyperosmotic stress response and exhibited increased translation and/or abundance during the late osmoadaptive phase (Figure S5B). The increase in *HSPB8* mRNA abundance and translational efficiency was confirmed by polysome profiling/qRT-PCR (Figures S3C–S3D). We also verified that these changes in *HSPB8* mRNA abundance and translational efficiency were accompanied by an increase in protein levels (Figure S3E). Importantly, two chaperone-encoding mRNAs known to participate in restoration of cell volume and morphology (Loyher et al., 2004) showed a biphasic response: translation of *HSPB11* mRNA was increased during the early phase (1 h of mild hyperosmotic stress) but reversed during the osmoadaptive phase (6 h of mild hyperosmotic stress), whereas *HSPG2* mRNA translation was suppressed during the early phase followed by translational activation during osmoadaptation (Figure S5B). Finally, the HSPA4L chaperone that promotes osmotolerance (Held et al., 2006) was translationally induced during osmoadaptation (Figure S5B). In summary, these gene-expression patterns are in agreement with the idea that osmoadaptation involves reprogramming of gene expression to protect cells from protein aggregation.

SNAT2 governs the biphasic translation program

We next asked whether mTOR mediates the effects of SNAT2 on early phase and osmoadaptation-induced translatomes. We performed ribosome profiling in cells where SNAT2 or mTOR activities were inhibited for the last hour of the osmoadaptive phase (during the last hour of 6 h 500 mOsm treatment) using MeAIB or torin 1, respectively (Figures 3A and S3F–S3G). MeAIB inhibited p70S6K phosphorylation by 70%, in contrast to near-complete inhibition by torin 1 (Figures S3F–S3G). GADD34 levels were not affected by MeAIB or torin 1 treatments (Figure S3F). Despite both inhibitors exerting only marginal effects on mRNA abundance (Figures 4A and 4B), both MeAIB and torin 1 dramatically perturbed translation (Figures 4A and 4B). To assess the contribution of mTOR to SNAT2-directed translational reprogramming, we contrasted the effects of MeAIB and torin 1 in treated cells. Only 35 out of 242 transcripts (14%) whose translation was suppressed by MeAIB were also translationally suppressed by torin 1 (Figure 4C), suggesting that the effects of SNAT2 on translation are, in part, independent of mTOR. To assess this unexpected observation, we studied how transcripts whose translation was
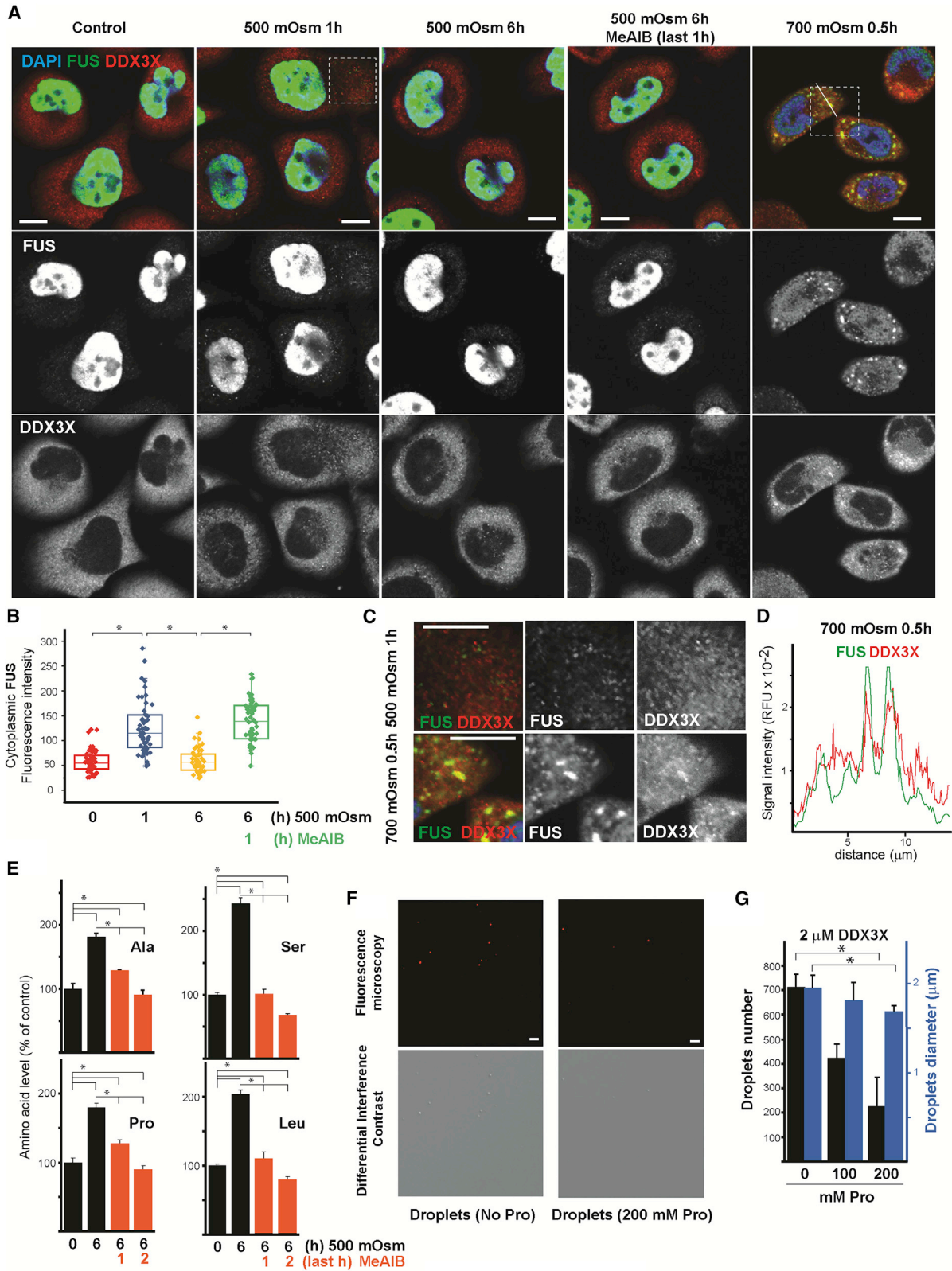
suppressed by MeAIB were regulated during the early and late phases. Strikingly, although these transcripts largely showed the biphasic translation pattern during the early versus late phases, their translation was only marginally affected by torin 1 (Figures 4E and S6). Specifically, 91% of mRNAs whose translation decreased following MeAIB treatment were also translationally suppressed during the early stress phase (Figure 4G), while 82% of these mRNAs were translationally activated during the osmoadaptive phase (Figure 4H). In addition, transcripts translationally activated upon MeAIB treatment (Figure 4A) partially overlapped with mRNAs whose translation was induced by torin 1 (42 out of 80; 52%; Figure 4C) and showed the biphasic translation pattern (Figure 4E), while 79% overlapped with mRNAs whose translation was stimulated during the early stress phase (Figures 4G), and 83% were translationally repressed during the late phase (Figure 4H). Consistent with mTOR-independent modulation of translation by SNAT2, mRNAs translationally suppressed by torin 1 were largely unaffected by MeAIB (Figures 4F and S7). In contrast, transcripts that were translationally activated by torin 1 were translationally suppressed during osmoadaptation while not being translationally activated during the early phase (Figures 4F, 4I–4J, and S7). To further investigate the potential implication of mTOR in osmoadaptive translation, we monitored the activity of oligopyrimidine tract (TOP motif)-containing mRNAs sensitive to modulation of mTOR activity (Thoreen et al., 2012; Ban et al., 2014). In agreement with the perturbations in mTOR activity, TOP mRNAs were translationally suppressed during early hyperosmotic stress, and their translation was partially recovered during the osmoadaptive phase (Figures S3A and S8). Notably, TOP mRNA translation was only marginally affected by MeAIB. Collectively, these data demonstrate that SNAT2 mediates osmoadaptive translation programs at least in part independently of mTOR.

RNA features that mediate biphasic regulation of translation during hyperosmotic stress

To further establish mechanisms underpinning translation perturbations during osmoadaptation, we next sought to identify shared features among mRNAs affected by mild hyperosmotic stress. We found mRNAs translationally suppressed during acute mild stress had higher G/C content (Figures S13A–S13C) relative to translationally activated mRNAs. Consistent with the biphasic translation program, higher G/C content was enriched among transcripts translationally activated after 6 h of stress compared with those activated during the acute stress phase (Figures S9A–S9C). Strikingly, the relationship between changes in translational efficiency and G/C content was nearly linear (Figures S9A–S9C). Therefore, 5′ UTR G/C content may associate with the biphasic translation program observed during hyperosmotic stress. Importantly, mRNAs that were translationally suppressed by either torin 1 or MeAIB also showed higher G/C content compared with unaffected or translationally upregulated transcripts (Figures S9D–S9F).

(F) Scatterplots as in (E) assessing how transcripts exhibiting torin 1-sensitive translation (B) are regulated under early (1 h 500 mOsm; bottom left) or adaptive (6 h 500 mOsm) phases in the absence (bottom center) or presence (bottom right) of MeAIB.

(G–J) Pie charts as described in Figure 3D showing how transcripts whose translation is altered by MeAIB (G and H) or torin 1 (I and J) treatment were regulated during early (G and I) or adaptive (H and J) stress phases.

A

Control | 500 mOsm 1h | 500 mOsm 6h | 500 mOsm 6h MeAIB (last 1h) | 700 mOsm 0.5h

DAPI FUS DDX3X

FUS

DDX3X

B

Cytoplasmic FUS Fluorescence intensity

0   1   6   6   (h) 500 mOsm
              1   (h) MeAIB

C

500 mOsm 1h: FUS DDX3X | FUS | DDX3X

700 mOsm 0.5h: FUS DDX3X | FUS | DDX3X

D

700 mOsm 0.5h
FUS DDX3X

Signal intensity (RFU x 10⁻²)

distance (μm)

E

Amino acid level (% of control)

Ala | Ser

Pro | Leu

0   6   6   6   (h) 500 mOsm
        1   2   (last h) MeAIB

F

Fluorescence microscopy

Differential Interference Contrast

Droplets (No Pro) | Droplets (200 mM Pro)

G

2 μM DDX3X

Droplets number / Droplets diameter (μm)

0   100   200
mM Pro

(legend on next page)

Mild stress induces SNAT2-mediated reversible formation of cytoplasmic FUS and DDX3X condensates

While RNA features underlying mTOR-sensitive translation have been described (Masvidal et al., 2017), factors underlying SNAT2-dependent translation are unknown. The high G/C content of mRNAs showing MeAIB-inhibited translation suggests changes in the interaction of RNA helicases with these mRNAs under hyperosmotic stress conditions (Bourgeois et al., 2016; Shen and Pelletier, 2020). Furthermore, cells often form cytoplasmic membraneless stress granules (SGs) in response to diverse environmental stress conditions (Hofmann et al., 2021; Ripin and Parker, 2022). Recently it was suggested that these "biological condensates" may involve transient interactions of scaffold RBPs with complexes facilitating formation of multisubunit complexes (Cech, 2022; Chen and Mayr, 2022). Due to its prominence in the literature, we investigated the RBP FUS, as in response to hyperosmotic stress, neurons show cytoplasmic localization of FUS in granules (Hock et al., 2018). Furthermore, cytoplasmic mutant FUS accumulation in neurons alters mRNA translation (Kamelgarn et al., 2018). The RNA helicase DDX3X promotes translation of mRNAs with long and G/C-rich 5′ UTRs (Lee et al., 2008) and is an SG component (Hilliker et al., 2011). Moreover, *DDX3X* was among those mRNAs translationally induced during the early phase, followed by an increase in mRNA levels during the late osmoadaptive phase (Figure 3E). We therefore tested the hypothesis that the activity of SNAT2 may affect formation of FUS and DDX3X condensates during the progression to osmoadaptation. We observed increased cytoplasmic FUS inclusions during the early mild-hyperosmotic-stress-response phase in corneal epithelial cells, which decreased during osmoadaptation (Figures 5A and 5B). Of note, in HeLa cells, high-intensity hyperosmotic stress (700 mOsm) results in exclusion of FUS from the nucleus and accumulation in SGs (Sama et al., 2013), in stark contrast to hyperosmotic-stress-induced FUS translocation in neurons that is independent of SGs (Hock et al., 2018). Importantly, during the early phase, there was no significant colocalization of FUS and the Ras-GAP-SH3-domain-binding protein 1 (G3BP1), a marker for SGs (Alam and Kennedy, 2019) (Figure S10A). In contrast, 1 h exposure to extreme hyperosmotic stress caused FUS colocalization with G3BP1 (Figure S10B) similar to that observed upon heat shock (Figure S10C). These results suggest that the biphasic response of osmoadaptation involves transient formation of FUS cytoplasmic inclusions, distinct from SGs. The distinct nature of FUS inclusions in mild stress was further supported by the absence of FUS/DDX3X colocalization during the early phase of the mild hyperosmotic-stress response

(Figures 5A, 5C and 5D). As expected, DDX3X colocalized with G3BP1 during heat shock (Figure S10C) and 700 mOsm stress (Figure S10D). The observed differences in RBP colocalization in condensates with increasing stress intensity supports the idea of stress-intensity-mediated remodeling of complexes in these condensates via RNA scaffolding proteins yet to be identified (Chen and Mayr, 2022). Taken together, the SNAT2-mediated translational reprogramming in adaptation to mild hyperosmotic stress appears to correlate with transient induction of FUS and DDX3X cytoplasmic condensates.

We next tested the role of SNAT2 in reversing the formation of these cytoplasmic condensates during osmoadaptation by inhibiting SNAT2 activity during the last hour of a 6 h treatment with MeAIB. Interestingly, MeAIB-treated cells sustained inclusions with both proteins during the osmoadaptive phase (Figures 5A, 5B, and 6A–6B). As amino acids and their derivatives can prevent protein aggregation (Shiraki et al., 2002), we next tested whether acute SNAT2 inhibition during osmoadaptation altered the intracellular amino acid pool. Acute inhibition of SNAT2 activity with MeAIB for the last hour of treatment decreased the amino acid levels, comparable to genetic inactivation of SNAT2 (Figures 5E and 2F). A recent report identified Pro as the driver in the adaptive transitioning to otherwise lethal intensity of hypertonic challenge (Thiemicke and Neuert, 2021). Pro levels decreased when cells were treated with MeAIB during the osmoadaptation phase (Figure 5E). These findings motivated us to test the ability of Pro to reverse condensates of liquid-liquid phase separation (LLPS) droplet formation *in vitro*. We show that Pro inhibited assembly and the size of recombinant DDX3X droplets (Figures 5F and 5G). Taken together, these data suggest a model whereby SNAT2-mediated accumulation of Pro and other amino acids during the osmoadaptive phase disassembles FUS and DDX3X condensates assembled during the early phase (Figures 5B and 6B).

Further supporting a role of FUS in the biphasic translation program, we identified FUS-binding sites as enriched among mRNAs translationally repressed during the early phase and recovered during osmoadaptation (Figures S10E–S10F). Moreover, mRNAs whose translation was suppressed by MeAIB, but not torin 1, were enriched for FUS motifs (Figure S10G), consistent with previous studies showing that FUS mutants repress translation of a subset of mRNAs in neurons (Birsa et al., 2021). Collectively, these findings suggest that FUS likely plays a role in SNAT2-dependent translation reprograming during mild hyperosmotic stress.

Our findings also suggest that early mild hyperosmotic stress induces formation of DDX3X condensates resolved

Figure 5. Distinct cytoplasmic FUS and DDX3X inclusions signify progression to osmoadaptation

(A–E) NaCl was used as an osmolyte.

(A) Subcellular distribution of FUS and DDX3X in corneal cells exposed to 500 or 700 mOsm media for the indicated times. Scale bars: 10 μm

(B) Quantification of cytoplasmic FUS inclusions in cells exposed to 500 mOsm media. MeAIB was added during the last 1 h of 6 h treatment. n > 52, error bars represent SEM, p < 0.01, Tukey's range test (from two-way ANOVA).

(C) Magnification of the area indicated in (A) from cells treated with the indicated osmolarity. Scale bars: 10 μm

(D) Analysis of FUS and DDX3X intensity along the line indicated in (A) from cells treated with 700 mOsm.

(E) Changes in levels of the indicated amino acids after inhibition of SNAT2 with MeAIB. n = 3, error bars represent SEM, *p < 0.01; n.s., not significant.

(F) Representative image of DDX3X droplets under fluorescent microscopy and differential interference contrast (DIC). Scale bars: 10 μm

(G) Droplet number and diameter formed by the DDX3X protein in solution following addition of Pro . Error bars represent SEM, *p < 0.01.
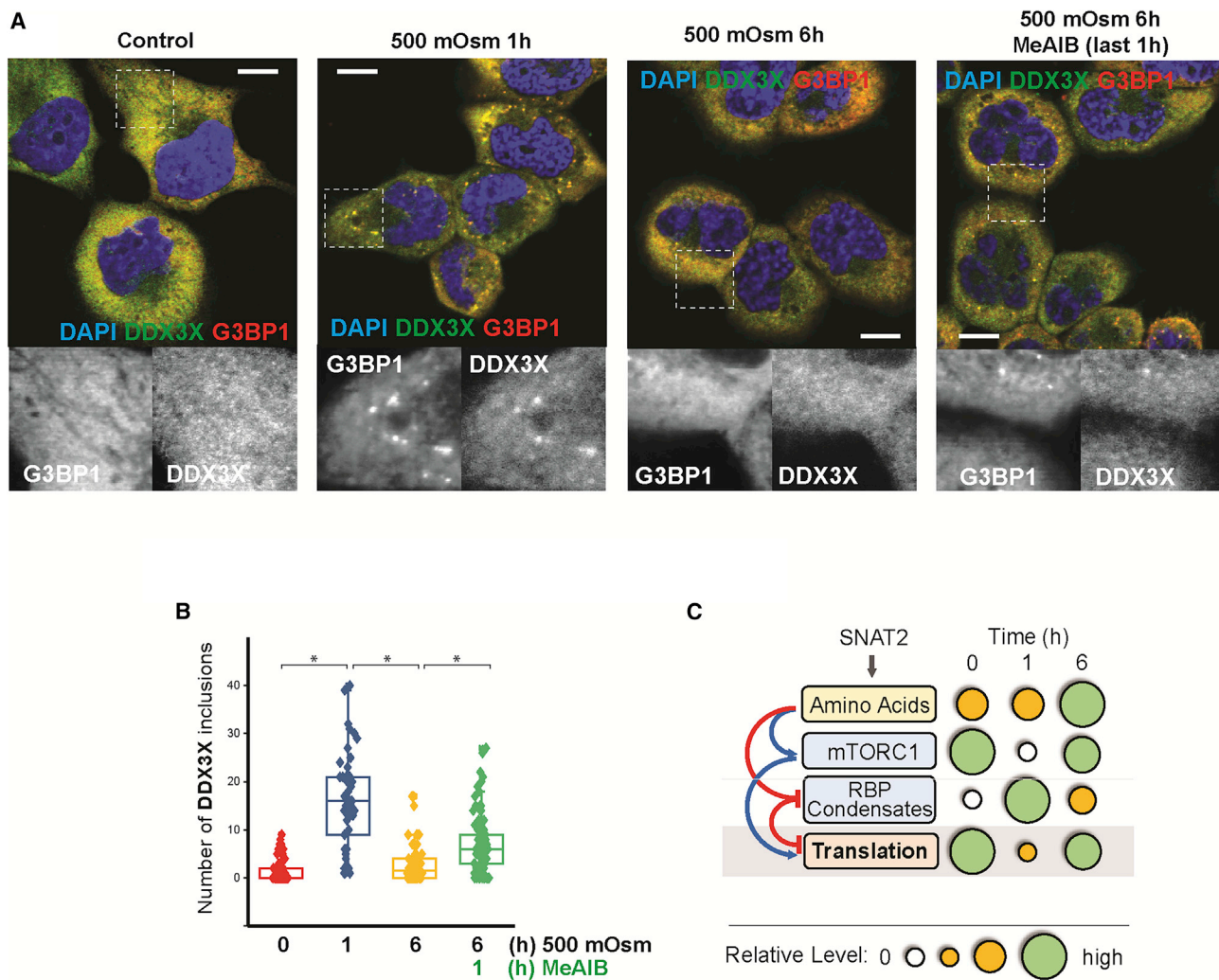
Figure 6. Hyperosmotic-stress-induced DDX3X colocalization with G3BP1 is resolved during osmoadaptation dependent on SNAT2 activity
(A and B) NaCl was used as an osmolyte.
(A) Immunofluorescence msicroscopy for the indicated proteins and cell treatments. Dotted squares indicate regions of magnified images shown. Scale bars: 10 μm
(B) Quantification of cytoplasmic DDX3X condensates in cells exposed to 500 mOsm media for the indicated times. MeAIB was added for the last 1 h of 6 h 500 mOsm treatment. n > 46, error bars represent SEM, p < 0.01, Tukey's range test (from two-way ANOVA).
(C) Proposed model of SNAT2-mediated translational reprogramming in osmoadaptation. Mild hyperosmotic stress induces biphasic translational control. In the early response (phase 1, 1 h of stress), macromolecular crowding, decreased protein diffusion, and changes in the cytoskeleton cause (1) decreased mTOR activity and global translation inhibition and (2) increased levels of FUS and DDX3X cytoplasmic condensates correlated with translation inhibition. In the late osmoadaptive phase (phase 2, 6 h of stress), increased expression of SNAT2 leads to accumulation of amino acids that reverse mTOR and global protein synthesis inhibition. Accumulated amino acids function as chemical chaperones to reverse formation of RBP condensates. Bubble sizes reflect overall activity level (mTORC1, translation), overall levels (amino acids), and size of effect (cytoplasmic RBP condensates) relative to maximal observed values.

during the osmoadaptive phase (Figures 6A and 6B). Strikingly, mRNAs that exhibit biphasic translational responses under mild hyperosmotic stress were enriched for those translationally stimulated by DDX3X (Calviello et al., 2021), and these effects were reversed during osmoadaptation (Figure S10H). These data suggest that DDX3X may change the mode of association with target mRNAs in condensates during the early phase, which would lead to their suppressed translation (Figures 6B and S10H). Importantly, this regulation is independent of eIF2α phosphorylation (Sidrauski et al., 2015). A similar

observation was made for a mutant DDX3X protein that can form condensates and cause translational repression independent of eIF2α phosphorylation (Valentin-Vega et al., 2016). Similar to that observed for FUS, there was a significant overlap between DDX3X-sensitive mRNAs and those translationally modulated by MeAIB but not by torin 1 (Figure S10I). While future studies are required to determine the precise function of FUS and DDX3X, our data suggest that these proteins mediate the effects of SNAT2 on mRNA translation during mild hyperosmotic stress.

CellPress
OPEN ACCESS

DISCUSSION

The molecular underpinnings of osmoadaptation remain poorly understood. Herein, we characterized the biphasic response to mild hyperosmotic stress. We show that the hallmarks of the early phase of the hyperosmotic-stress response are suppression of mTOR, reduction in global protein synthesis, and translation reprogramming, including induction of SNAT2. The late osmoadaptation phase is characterized by increased SNAT2 activity, partial restoration of mTOR signaling, and reshaping of the early-phase translatome. Notably, the mechanism of the translation reprogramming during osmoadaptation includes the coordinated but independent activities of SNAT2 and mTOR. In addition, we show the SNAT2-dependent biphasic response to mild hyperosmotic stress may involve FUS and DDX3X condensates (Figure 6C).

Similar to the ISR, mild hyperosmotic stress inhibits global protein synthesis; however, unlike the ISR, this is independent of eIF2α signaling. Transcripts preferentially translated during the early phase of the mild hyperosmotic-stress response encode osmoprotective proteins SNAT2 and TonEBP (Burg et al., 2007). This is followed by an osmoadaptive phase, characterized by translation of mRNAs encoding osmoprotective proteins and partial reversal of translation programs established during the early phase. In contrast, prolonged ISR largely involves sustained early-phase translational reprogramming. Thus, there are fundamental differences between mechanisms underpinning these biphasic stress responses.

We show here that SNAT2 provides Gln to the exchanger LAT1 (SLC7A5), leading to increased accumulation of BCAAs during osmoadaptation. This increase in BCAAs correlates with mTOR reactivation (Takahara et al., 2020), suggesting that osmoadaptation involves communication between SNAT2 and LAT1 via their common substrate Gln. Similar coordination of transporter activity occurs in disease-related systems (Bott et al., 2015). The accumulation of osmolytes in response to hyperosmotic stress also reverses protein aggregation in the early phase (Burg et al., 2007). Osmolytes can protect and stabilize proteins by thermodynamically modulating unfolded states (Yancey et al., 1982). Our data support a model whereby SNAT2 acts as a molecular switch between the early response of protein aggregation and its reversal in the late osmoadaptive response via the accumulation of amino acids.

We identified several heat shock proteins (HSPs) that are translationally regulated during the biphasic response to the mild hyperosmotic stress. Translation of *HSPB8* during the early phase of hyperosmotic stress and induction of mRNA in the osmoadaptive phase are consistent with the function of HSPB8 in inhibiting protein aggregation (Ganassi et al., 2016). It was recently shown that HSPB8 may also stabilize the aggregation-prone RNA-binding domain of FUS and thus prevent FUS aggregation (Boczek et al., 2021). Stress-induced phosphorylation of HSP27, another small HSP (SHSP) that protects cells from hyperosmotic stress (Head et al., 1994), has been linked to preservation of LLPS by FUS, inhibiting irreversible aggregate formation (Liu et al.,

2020). HSP27 phosphorylation is increased during the early response to hyperosmotic stress (Liu et al., 2020), consistent with the reversibility of FUS inclusions. Based on these findings, we propose that SHSPs are essential osmoprotectants required for the transition to osmoadaptation.

Our studies suggest an involvement of non-overlapping FUS and DDX3X condensates in the biphasic response to hyperosmotic stress. This can be explained by a recent report (Kar et al., 2022) demonstrating that at sub-saturation concentrations, RBPs with disordered domains, such as FUS, can form sequence-specific clusters distinct from phase separation observed in supersaturated concentrations. Those authors suggest that solutes can influence coupling and uncoupling of phase behaviors, in agreement with our findings that SNAT2-related amino acid uptake can regulate this process. Although we show colocalization of SG components DDX3X and G3BP1 (Hilliker et al., 2011; Hofmann et al., 2021), additional studies are required to determine their composition and similarities with SGs. As it does not colocalize with SG markers, FUS may be involved either in translation suppression of mRNAs that contain FUS-binding sites or act as a scaffolding protein to form condensates (Guo et al., 2021). The reversible assembly of stress-induced condensates during the progression to osmoadaptation raises questions regarding the mechanisms of their assembly and disassembly. We speculate that stress-induced cytoskeleton perturbations (Krokowski et al., 2017) and dehydration may generate RBP condensates during the acute phase of hyperosmotic stress.

Furthermore, increased levels of chaperones may maintain condensate dynamics. Protein chaperones, RNA helicases, and microtubule dynamics have been reported to be important for SG disassembly (Mateju et al., 2017; van Ommen et al., 1989). We highlight an additional component for disassembly of stress-induced condensates: amino acid accumulation by SNAT2 during osmoadaptation. Although the mechanism of amino-acid-mediated disassembly is not clear, the phenomenon is reminiscent of studies in yeast showing metabolite-mediated disassembly of SGs in response to heat shock. When cells are placed in a heat-stress-free environment, fructose-1,6-bisphosphate accumulates in SGs and promotes disassembly of SGs (Cereghetti et al., 2021). It is therefore possible that amino acids and chaperones form a network maintaining condensates during osmoadaptation in response to mild stress. It was previously shown that hyperosmolar conditions induce LLPS (Watanabe et al., 2021; Yasuda et al., 2020; Olins et al., 2020). In addition, the ATP-bound form of DDX3X promotes LLPS (Hondele et al., 2019). It is therefore plausible that DDX3X is an important component of LLPS during osmoadaptation. Future research is warranted to determine the mechanisms and functions of FUS and DDX3X in osmoadaptation.

In conclusion, our data demonstrate that SNAT2 plays a central role in the transition from the early hyperosmotic-stress response to osmoadaptation. Many studies have shown that under physiological conditions, the kidneys, cornea, liver, intervertebral discs, gastrointestinal tract, and joints are exposed to hyperosmotic fluids (Brocker et al., 2012). An increase from the physiological 300 mOsm tonicity to 343 mOsm is sufficient to

cause dry eye syndrome (Baudouin et al., 2013). Considering that the inability to adapt to mild hyperosmotic stress can lead to an inflammatory response and cell death (Farabaugh et al., 2020), our studies on the biphasic response in establishing osmoadaptation to mild hyperosmotic stress may initiate new paradigms to protect osmosensitive tissues.

Limitations of the study

The mechanism(s) of how amino acids disassemble RBP condensates during osmoadaptation remains unclear. Potential mechanisms may be revealed using *in vitro* systems of LLP formation and by testing assembly and disassembly of droplets by individual amino acids in the presence/absence of RNA and/or small heat shock chaperone proteins. In addition, we do not know if and which mRNAs bind to identified RBPs showing SNAT2-dependent disassembly. This question can be addressed by performing cross-linking immunoprecipitation experiments to identify the mRNAs and kinetics of binding of the RBPs to subsets of mRNAs during the biphasic response to hyperosmotic stress.

STAR★METHODS

Detailed methods are provided in the online version of this paper and include the following:

- KEY RESOURCES TABLE
- RESOURCE AVAILABILITY
  - Lead contact
  - Materials availability
  - Data and code availability
- EXPERIMENTAL MODEL AND SUBJECT DETAILS
  - Cell lines, cell culture treatments and chemicals
- METHOD DETAILS
  - Protein extraction and western blot analysis
  - Gene knockdown experiments
  - Generation of SLC38A2 knock-out cell line using CRISPR-CAS9
  - Amino acid uptake assays
  - Measurement of protein synthesis rates via puromycin incorporation and metabolic labeling with [35S]-Met/Cys
  - Measuring *in vitro* guanine nucleotide exchange factor (GEF) activity of eIF2B
  - Amino acid analysis
  - Ribosome footprinting analysis
  - Cytoplasmic RNA levels
  - Ribosomal footprinting data analysis
  - RNA-seq data analysis
  - Analysis of differential translation with anota2seq
  - Motif discovery
  - mRNA's general features analysis
  - Polysome profile and qPCR analysis
  - Microscopy
  - DDX3X purification
  - *In vitro* phase separation of DDX3X
- QUANTIFICATION AND STATISTICAL ANALYSIS

AUTHOR CONTRIBUTIONS

Project conceptualization, D.K. and M.H.; methodology development, R.J., Z.G., Y.M., P.R., H.M., and S.-B.Q.; investigation, D.K., R.J., K.J.S., C.-W.C., B.-J.G., J.W., X.F., S.V., and W.B.; bioinformatics, K.S., A.I.S., and O.L.; resources, M.M., N.T.K., A.V., W.C.M., E.J., M.T., and T.M.; data curation, D.K., R.J., K.J.S., C.-W.C., I.T., O.L., and M.H.; writing, D.K., O.L., I.T., and M.H.; review & editing, all authors; visualization, D.K., B.-J.G., and K.J.S.; funding acquisition, D.K., I.T., O.L., and M.H.; supervision, M.H.

REFERENCES

Alam, U., and Kennedy, D. (2019). Rasputin a decade on and more promiscuous than ever? A review of G3BPs. Biochim. Biophys. Acta Mol. Cell Res. *1866*, 360–370. https://doi.org/10.1016/j.bbamcr.2018.09.001.

Al-Baghdadi, R.J.T., Nikonorova, I.A., Mirek, E.T., Wang, Y., Park, J., Belden, W.J., Wek, R.C., and Anthony, T.G. (2017). Role of activating transcription factor 4 in the hepatic response to amino acid depletion by asparaginase. Sci. Rep. *7*, 1272. https://doi.org/10.1038/s41598-017-01041-7.

Anders, S., Pyl, P.T., and Huber, W. (2015). HTSeq–a Python framework to work with high-throughput sequencing data. Bioinformatics *31*, 166–169. https://doi.org/10.1093/bioinformatics/btu638.

Bailey, T.L. (2011). DREME: motif discovery in transcription factor ChIP-seq data. Bioinformatics *27*, 1653–1659. https://doi.org/10.1093/bioinformatics/btr261.

Bailey, T.L., Boden, M., Buske, F.A., Frith, M., Grant, C.E., Clementi, L., Ren, J., Li, W.W., and Noble, W.S. (2009). MEME SUITE: tools for motif discovery and searching. Nucleic Acids Res. *37*, W202–W208. https://doi.org/10.1093/nar/gkp335.

Baird, T.D., and Wek, R.C. (2012). Eukaryotic initiation factor 2 phosphorylation and translational control in metabolism. Adv. Nutr. *3*, 307–321. https://doi.org/10.3945/an.112.002113.

Ban, N., Beckmann, R., Cate, J.H., Dinman, J.D., Dragon, F., Ellis, S.R., Lafontaine, D.L., Lindahl, L., Liljas, A., Lipton, J.M., et al. (2014). A new system for naming ribosomal proteins. Curr. Opin. Struct. Biol. *24*, 165–169. https://doi.org/10.1016/j.sbi.2014.01.002.

Baudouin, C., Aragona, P., Messmer, E.M., Tomlinson, A., Calonge, M., Boboridis, K.G., Akova, Y.A., Geerling, G., Labetoulle, M., and Rolando, M. (2013). Role of hyperosmolarity in the pathogenesis and management of dry

eye disease: proceedings of the OCEAN group meeting. Ocul. Surf. *11*, 246–258. https://doi.org/10.1016/j.jtos.2013.07.003.

Bevilacqua, E., Bussolati, O., Dall'Asta, V., Gaccioli, F., Sala, R., Gazzola, G.C., and Franchi-Gazzola, R. (2005). SNAT2 silencing prevents the osmotic induction of transport system A and hinders cell recovery from hypertonic stress. FEBS Lett. *579*, 3376–3380. https://doi.org/10.1016/j.febslet.2005.05.002.

Bindea, G., Mlecnik, B., Hackl, H., Charoentong, P., Tosolini, M., Kirilovsky, A., Fridman, W.H., Pagès, F., Trajanoski, Z., and Galon, J. (2009). ClueGO: a Cytoscape plug-in to decipher functionally grouped gene ontology and pathway annotation networks. Bioinformatics *25*, 1091–1093. https://doi.org/10.1093/bioinformatics/btp101.

Birsa, N., Ule, A.M., Garone, M.G., Tsang, B., Mattedi, F., Chong, P.A., Humphrey, J., Jarvis, S., Pisiren, M., Wilkins, O.G., et al. (2021). FUS-ALS mutants alter FMRP phase separation equilibrium and impair protein translation. Sci. Adv. *7*, eabf8660. https://doi.org/10.1126/sciadv.abf8660.

Boczek, E.E., Fürsch, J., Niedermeier, M.L., Jawerth, L., Jahnel, M., Ruer-Gruss, M., Kammer, K.M., Heid, P., Mediani, L., Wang, J., et al. (2021). HspB8 prevents aberrant phase transitions of FUS by chaperoning its folded RNA-binding domain. Elife *10*, e69377. https://doi.org/10.7554/elife.69377.

Bott, A.J., Peng, I.C., Fan, Y., Faubert, B., Zhao, L., Li, J., Neidler, S., Sun, Y., Jaber, N., Krokowski, D., et al. (2015). Oncogenic myc induces expression of glutamine synthetase through promoter demethylation. Cell Metabol. *22*, 1068–1077. https://doi.org/10.1016/j.cmet.2015.09.025.

Bourgeois, C.F., Mortreux, F., and Auboeuf, D. (2016). The multiple functions of RNA helicases as drivers and regulators of gene expression. Nat. Rev. Mol. Cell Biol. *17*, 426–438. https://doi.org/10.1038/nrm.2016.50.

Brocker, C., Thompson, D.C., and Vasiliou, V. (2012). The role of hyperosmotic stress in inflammation and disease. Biomol. Concepts *3*, 345–364. https://doi.org/10.1515/bmc-2012-0001.

Broer, A., Rahimi, F., and Bröer, S. (2016). Deletion of amino acid transporter ASCT2 (SLC1A5) reveals an essential role for transporters SNAT1 (SLC38A1) and SNAT2 (SLC38A2) to sustain glutaminolysis in cancer cells. J. Biol. Chem. *291*, 13194–13205. https://doi.org/10.1074/jbc.m115.700534.

Broer, S. (2014). The SLC38 family of sodium-amino acid co-transporters. Pflueg. Arch. Eur. J. Physiol. *466*, 155–172. https://doi.org/10.1007/s00424-013-1393-y.

Burg, M.B., Ferraris, J.D., and Dmitrieva, N.I. (2007). Cellular response to hyperosmotic stresses. Physiol. Rev. *87*, 1441–1474. https://doi.org/10.1152/physrev.00056.2006.

Burg, M.B., Kwon, E.D., and KÜltz, D. (1997). Regulation of gene expression by hypertonicity. Annu. Rev. Physiol. *59*, 437–455. https://doi.org/10.1146/annurev.physiol.59.1.437.

Bussolati, O., Dall'Asta, V., Franchi-Gazzola, R., Sala, R., Rotoli, B.M., Visigalli, R., Casado, J., Lopez-Fontanals, M., Pastor-Anglada, M., and Gazzola, G.C. (2001). The role of system A for neutral amino acid transport in the regulation of cell volume. Mol. Membr. Biol. *18*, 27–38. https://doi.org/10.1080/09687680110033756.

Calviello, L., Mukherjee, N., Wyler, E., Zauber, H., Hirsekorn, A., Selbach, M., Landthaler, M., Obermayer, B., and Ohler, U. (2016). Detecting actively translated open reading frames in ribosome profiling data. Nat. Methods *13*, 165–170. https://doi.org/10.1038/nmeth.3688.

Calviello, L., Venkataramanan, S., Rogowski, K.J., Wyler, E., Wilkins, K., Tejura, M., Thai, B., Krol, J., Filipowicz, W., Landthaler, M., and Floor, S. (2021). DDX3 depletion represses translation of mRNAs with complex 5' UTRs. Nucleic Acids Res. *49*, 5336–5350. https://doi.org/10.1093/nar/gkab287.

Cech, T.R. (2022). RNA in biological condensates. RNA *28*, 1–2. https://doi.org/10.1261/rna.079051.121.

Cereghetti, G., Wilson-Zbinden, C., Kissling, V.M., Diether, M., Arm, A., Yoo, H., Piazza, I., Saad, S., Picotti, P., Drummond, D.A., et al. (2021). Reversible amyloids of pyruvate kinase couple cell metabolism and stress granule disassembly. Nat. Cell Biol. *23*, 1085–1094. https://doi.org/10.1038/s41556-021-00760-4.

Chen, X., and Mayr, C. (2022). A working model for condensate RNA-binding proteins as matchmakers for protein complex assembly. RNA *28*, 76–87. https://doi.org/10.1261/rna.078995.121.

Costa-Mattioli, M., and Walter, P. (2020). The integrated stress response: from mechanism to disease. Science *368*, eaat5314. https://doi.org/10.1126/science.aat5314.

Darnell, A.M., Subramaniam, A.R., and O'Shea, E.K. (2018). Translational control through differential ribosome pausing during amino acid limitation in mammalian cells. Mol. Cell *71*, 229–243.e11. https://doi.org/10.1016/j.molcel.2018.06.041.

Eveloff, J.L., and Warnock, D.G. (1987). Activation of ion transport systems during cell volume regulation. Am. J. Physiol. *252*, F1–F10. https://doi.org/10.1152/ajprenal.1987.252.1.f1.

Farabaugh, K.T., Krokowski, D., Guan, B.J., Gao, Z., Gao, X.H., Wu, J., Jobava, R., Ray, G., de Jesus, T.J., Bianchi, M.G., et al. (2020). PACT-mediated PKR activation acts as a hyperosmotic stress intensity sensor weakening osmoadaptation and enhancing inflammation. Elife *9*, e52241. https://doi.org/10.7554/elife.52241.

Feleciano, D.R., Juenemann, K., Iburg, M., Brás, I.C., Holmberg, C.I., and Kirstein, J. (2019). Crosstalk between chaperone-mediated protein disaggregation and proteolytic pathways in aging and disease. Front. Aging Neurosci. *11*, 9. https://doi.org/10.3389/fnagi.2019.00009.

Ferraris, J.D., and Burg, M.B. (2006). Tonicity-dependent regulation of osmoprotective genes in mammalian cells. Contrib. Nephrol. *152*, 125–141. https://doi.org/10.1159/000096320.

Franchi-Gazzola, R., Dall'Asta, V., Sala, R., Visigalli, R., Bevilacqua, E., Gaccioli, F., Gazzola, G.C., and Bussolati, O. (2006). The role of the neutral amino acid transporter SNAT2 in cell volume regulation. Acta Physiol. *187*, 273–283. https://doi.org/10.1111/j.1748-1716.2006.01552.x.

Franchi-Gazzola, R., Gaccioli, F., Bevilacqua, E., Visigalli, R., Dall'Asta, V., Sala, R., Varoqui, H., Erickson, J.D., Gazzola, G.C., and Bussolati, O. (2004). The synthesis of SNAT2 transporters is required for the hypertonic stimulation of system A transport activity. Biochim. Biophys. Acta. *1667*, 157–166. https://doi.org/10.1016/j.bbamem.2004.09.012.

Franchi-Gazzola, R., Visigalli, R., Bussolati, O., Dall'Asta, V., and Gazzola, G.C. (1999). Adaptive increase of amino acid transport system A requires ERK1/2 activation. J. Biol. Chem. *274*, 28922–28928. https://doi.org/10.1074/jbc.274.41.28922.

FWolfson, R.L., Chantranupong, L., Saxton, R.A., Shen, K., Scaria, S.M., Cantor, J.R., and Sabatini, D.M. (2016). Sestrin2 is a leucine sensor for the mTORC1 pathway. Science *351*, 43–48. https://doi.org/10.1126/science.aab2674.

Ganassi, M., Mateju, D., Bigi, I., Mediani, L., Poser, I., Lee, H.O., Seguin, S.J., Morelli, F.F., Vinet, J., Leo, G., et al. (2016). A surveillance function of the HSPB8-BAG3-HSP70 chaperone complex ensures stress granule integrity and dynamism. Mol. Cell *63*, 796–810. https://doi.org/10.1016/j.molcel.2016.07.021.

Gerashchenko, M.V., and Gladyshev, V.N. (2014). Translation inhibitors cause abnormalities in ribosome profiling experiments. Nucleic Acids Res. *42*, e134. https://doi.org/10.1093/nar/gku671.

Guan, B.J., Krokowski, D., Majumder, M., Schmotzer, C.L., Kimball, S.R., Merrick, W.C., Koromilas, A.E., and Hatzoglou, M. (2014). Translational control during endoplasmic reticulum stress beyond phosphorylation of the translation initiation factor eIF2α. J. Biol. Chem. *289*, 12593–12611. https://doi.org/10.1074/jbc.m113.543215.

Guan, B.J., van Hoef, V., Jobava, R., Elroy-Stein, O., Valasek, L.S., Cargnello, M., Gao, X.H., Krokowski, D., Merrick, W.C., Kimball, S.R., et al. (2017). A unique ISR program determines cellular responses to chronic stress. Mol. Cell *68*, 885–900.e6. https://doi.org/10.1016/j.molcel.2017.11.007.

Guo, Q., Shi, X., and Wang, X. (2021). RNA and liquid-liquid phase separation. Non-Coding RNA Res. *6*, 92–99. https://doi.org/10.1016/j.ncrna.2021.04.003.

Gupta, S., Stamatoyannopoulos, J.A., Bailey, T.L., and Noble, W.S. (2007). Quantifying similarity between motifs. Genome Biol. *8*, R24. https://doi.org/10.1186/gb-2007-8-2-r24.

Han, J., Back, S.H., Hur, J., Lin, Y.H., Gildersleeve, R., Shan, J., Yuan, C.L., Krokowski, D., Wang, S., Hatzoglou, M., et al. (2013). ER-stress-induced transcriptional regulation increases protein synthesis leading to cell death. Nat. Cell Biol. *15*, 481–490. https://doi.org/10.1038/ncb2738.

Head, M.W., Corbin, E., and Goldman, J.E. (1994). Coordinate and independent regulation of alpha B-crystallin and hsp27 expression in response to physiological stress. J. Cell. Physiol. *159*, 41–50. https://doi.org/10.1002/jcp.1041590107.

Held, T., Paprotta, I., Khulan, J., Hemmerlein, B., Binder, L., Wolf, S., Schubert, S., Meinhardt, A., Engel, W., and Adham, I.M. (2006). Hspa4l-deficient mice display increased incidence of male infertility and hydronephrosis development. Mol. Cell Biol. *26*, 8099–8108. https://doi.org/10.1128/mcb.01332-06.

Hilliker, A., Gao, Z., Jankowsky, E., and Parker, R. (2011). The DEAD-box protein Ded1 modulates translation by the formation and resolution of an eIF4F-mRNA complex. Mol. Cell *43*, 962–972. https://doi.org/10.1016/j.molcel.2011.08.008.

Hinnebusch, A.G., Ivanov, I.P., and Sonenberg, N. (2016). Translational control by 5'-untranslated regions of eukaryotic mRNAs. Science *352*, 1413–1416. https://doi.org/10.1126/science.aad9868.

Hoch-Kraft, P., White, R., Tenzer, S., Krämer-Albers, E.M., Trotter, J., and Gonsior, C. (2018). Dual role of the RNA helicase DDX5 in post-transcriptional regulation of myelin basic protein in oligodendrocytes. J. Cell Sci. *131*, jcs204750. https://doi.org/10.1242/jcs.204750.

Hock, E.M., Maniecka, Z., Hruska-Plochan, M., Reber, S., Laferrière, F., Sahadevan, M.K.S., Ederle, H., Gittings, L., Pelkmans, L., Dupuis, L., et al. (2018). Hypertonic stress causes cytoplasmic translocation of neuronal, but not astrocytic, FUS due to impaired transportin function. Cell Rep. *24*, 987–1000.e7. https://doi.org/10.1016/j.celrep.2018.06.094.

Hoffmann, E.K., Lambert, I.H., and Pedersen, S.F. (2009). Physiology of cell volume regulation in vertebrates. Physiol. Rev. *89*, 193–277. https://doi.org/10.1152/physrev.00037.2007.

Hofmann, S., Kedersha, N., Anderson, P., and Ivanov, P. (2021). Molecular mechanisms of stress granule assembly and disassembly. Biochim. Biophys. Acta Mol. Cell Res. *1868*, 118876. https://doi.org/10.1016/j.bbamcr.2020.118876.

Hondele, M., Sachdev, R., Heinrich, S., Wang, J., Vallotton, P., Fontoura, B.M.A., and Weis, K. (2019). DEAD-box ATPases are global regulators of phase-separated organelles. Nature *573*, 144–148. https://doi.org/10.1038/s41586-019-1502-y.

Ingolia, N.T., Brar, G.A., Rouskin, S., McGeachy, A.M., and Weissman, J.S. (2012). The ribosome profiling strategy for monitoring translation in vivo by deep sequencing of ribosome-protected mRNA fragments. Nat Protoc 7, 1534–1550.

Ingolia, N.T., Ghaemmaghami, S., Newman, J.R.S., and Weissman, J.S. (2009). Genome-wide analysis in vivo of translation with nucleotide resolution using ribosome profiling. Science *324*, 218–223. https://doi.org/10.1126/science.1168978.

Jewell, J.L., Kim, Y.C., Russell, R.C., Yu, F.X., Park, H.W., Plouffe, S.W., Tagliabracci, V.S., and Guan, K.L. (2015). Differential regulation of mTORC1 by leucine and glutamine. Science *347*, 194–198. https://doi.org/10.1126/science.1259472.

Jobava, R., Mao, Y., Guan, B.J., Hu, D., Krokowski, D., Chen, C.W., Shu, X.E., Chukwurah, E., Wu, J., Gao, Z., et al. (2021). Adaptive translational pausing is a hallmark of the cellular response to severe environmental stress. Mol. Cell *81*, 4191–4208.e8. https://doi.org/10.1016/j.molcel.2021.09.029.

Kamelgarn, M., Chen, J., Kuang, L., Jin, H., Kasarskis, E.J., and Zhu, H. (2018). ALS mutations of FUS suppress protein translation and disrupt the regulation of nonsense-mediated decay. Proc. Natl. Acad. Sci. USA *115*, E11904–E11913. https://doi.org/10.1073/pnas.1810413115.

Kanai, Y., Stelzner, M.G., Lee, W.S., Wells, R.G., Brown, D., and Hediger, M.A. (1992). Expression of mRNA (D2) encoding a protein involved in amino acid transport in S3 proximal tubule. Am. J. Physiol. *263*, F1087–F1092. https://doi.org/10.1152/ajprenal.1992.263.6.f1087.

Kar, M., Dar, F., Welsh, T.J., Laura Vogel, L., Kühnemuth, R., Majumdar, A., Krainer, G., Franzmann, T.M., Alberti, S., Seidel, C.A.M., et al. (2022). Phase separating RNA binding proteins form heterogeneous distributions of clusters in subsaturated solutions. Preprint at bioRxiv. https://doi.org/10.1101/2022.02.03.478969.

Karunakaran, S., Ramachandran, S., Coothankandaswamy, V., Elangovan, S., Babu, E., Periyasamy-Thandavan, S., Gurav, A., Gnanaprakasam, J.P., Singh, N., Schoenlein, P.V., et al. (2011). SLC6A14 (ATB0, +) protein, a highly concentrative and broad specific amino acid transporter, is a novel and effective drug target for treatment of estrogen receptor-positive breast cancer. J. Biol. Chem. *286*, 31830–31838. https://doi.org/10.1074/jbc.m111.229518.

Kim, D., Langmead, B., and Salzberg, S.L. (2015). HISAT: a fast spliced aligner with low memory requirements. Nat. Methods *12*, 357–360. https://doi.org/10.1038/nmeth.3317.

Kimball, S.R., Everson, W.V., Flaim, K.E., and Jefferson, L.S. (1989). Initiation of protein synthesis in a cell-free system prepared from rat hepatocytes. Am. J. Physiol. *256*, C28–C34. https://doi.org/10.1152/ajpcell.1989.256.1.c28.

Klickstein, J.A., Mukkavalli, S., and Raman, M. (2020). AggreCount: an unbiased image analysis tool for identifying and quantifying cellular aggregates in a spatially defined manner. J. Biol. Chem. *295*, 17672–17683. https://doi.org/10.1074/jbc.ra120.015398.

Krokowski, D., Guan, B.J., Wu, J., Zheng, Y., Pattabiraman, P.P., Jobava, R., Gao, X.H., Di, X.J., Snider, M.D., Mu, T.W., et al. (2017). GADD34 function in protein trafficking promotes adaptation to hyperosmotic stress in human corneal cells. Cell Rep. *21*, 2895–2910. https://doi.org/10.1016/j.celrep.2017.11.027.

Krokowski, D., Han, J., Saikia, M., Majumder, M., Yuan, C.L., Guan, B.J., Bevilacqua, E., Bussolati, O., Bröer, S., Arvan, P., et al. (2013). A self-defeating anabolic program leads to beta-cell apoptosis in endoplasmic reticulum stress-induced diabetes via regulation of amino acid flux. J. Biol. Chem. *288*, 17202–17213. https://doi.org/10.1074/jbc.m113.466920.

Krokowski, D., Jobava, R., Guan, B.J., Farabaugh, K., Wu, J., Majumder, M., Bianchi, M.G., Snider, M.D., Bussolati, O., and Hatzoglou, M. (2015). Coordinated regulation of the neutral amino acid transporter SNAT2 and the protein phosphatase subunit GADD34 promotes adaptation to increased extracellular osmolarity. J. Biol. Chem. *290*, 17822–17837. https://doi.org/10.1074/jbc.m114.636217.

Lauria, F., Tebaldi, T., Bernabò, P., Groen, E.J.N., Gillingwater, T.H., and Viero, G. (2018). riboWaltz: optimization of ribosome P-site positioning in ribosome profiling data. PLoS Comput. Biol. *14*, e1006169. https://doi.org/10.1371/journal.pcbi.1006169.

Lee, C.S., Dias, A.P., Jedrychowski, M., Patel, A.H., Hsu, J.L., and Reed, R. (2008). Human DDX3 functions in translation and interacts with the translation initiation factor eIF3. Nucleic Acids Res. *36*, 4708–4718. https://doi.org/10.1093/nar/gkn454.

Liedtke, C.M., and Cole, T.S. (2002). Activation of NKCC1 by hyperosmotic stress in human tracheal epithelial cells involves PKC-delta and ERK. Biochim. Biophys. Acta. *1589*, 77–88. https://doi.org/10.1016/s0167-4889(01)00189-6.

Liu, Z., Zhang, S., Gu, J., Tong, Y., Li, Y., Gui, X., Long, H., Wang, C., Zhao, C., Lu, J., et al. (2020). Hsp27 chaperones FUS phase separation under the modulation of stress-induced phosphorylation. Nat. Struct. Mol. Biol. *27*, 363–372. https://doi.org/10.1038/s41594-020-0399-3.

Loyher, M.L., Mutin, M., Woo, S.K., Kwon, H.M., and Tappaz, M.L. (2004). Transcription factor tonicity-responsive enhancer-binding protein (TonEBP) which transactivates osmoprotective genes is expressed and upregulated following acute systemic hypertonicity in neurons in brain. Neuroscience *124*, 89–104. https://doi.org/10.1016/j.neuroscience.2003.10.025.

Maallem, S., Wierinckx, A., Lachuer, J., Kwon, M.H., and Tappaz, M.L. (2008). Gene expression profiling in brain following acute systemic hypertonicity: novel genes possibly involved in osmoadaptation.

J. Neurochem. *105*, 1198–1211. https://doi.org/10.1111/j.1471-4159.2008.05222.x.

Manifava, M., Smith, M., Rotondo, S., Walker, S., Niewczas, I., Zoncu, R., Clark, J., and Ktistakis, N.T. (2016). Dynamics of mTORC1 activation in response to amino acids. Elife *5*, e19960. https://doi.org/10.7554/elife.19960.

Mao, Y., Dong, L., Liu, X.M., Guo, J., Ma, H., Shen, B., and Qian, S.B. (2019). m(6)A in mRNA coding regions promotes translation via the RNA helicase-containing YTHDC2. Nat. Commun. *10*, 5332. https://doi.org/10.1038/s41467-019-13317-9.

Masvidal, L., Hulea, L., Furic, L., Topisirovic, I., and Larsson, O. (2017). mTOR-sensitive translation: cleared fog reveals more trees. RNA Biol. *14*, 1299–1305. https://doi.org/10.1080/15476286.2017.1290041.

Mateju, D., Franzmann, T.M., Patel, A., Kopach, A., Boczek, E.E., Maharana, S., Lee, H.O., Carra, S., Hyman, A.A., and Alberti, S. (2017). An aberrant phase transition of stress granules triggered by misfolded protein and prevented by chaperone function. EMBO J. *36*, 1669–1687. https://doi.org/10.15252/embj.201695957.

Nicklin, P., Bergman, P., Zhang, B., Triantafellow, E., Wang, H., Nyfeler, B., Yang, H., Hild, M., Kung, C., Wilson, C., et al. (2009). Bidirectional transport of amino acids regulates mTOR and autophagy. Cell *136*, 521–534. https://doi.org/10.1016/j.cell.2008.11.044.

Novoa, I., Zeng, H., Harding, H.P., and Ron, D. (2001). Feedback inhibition of the unfolded protein response by GADD34-mediated dephosphorylation of eIF2α. J. Cell Biol. *153*, 1011–1022. https://doi.org/10.1083/jcb.153.5.1011.

O'Connor, P.B., Andreev, D.E., and Baranov, P.V. (2016). Comparative survey of the relative impact of mRNA features on local ribosome profiling read density. Nat. Commun. *7*, 12915. https://doi.org/10.1038/ncomms12915.

Oertlin, C., Lorent, J., Murie, C., Furic, L., Topisirovic, I., and Larsson, O. (2019). Generally applicable transcriptome-wide analysis of translation using anota2seq. Nucleic Acids Res. *47*, e70. https://doi.org/10.1093/nar/gkz223.

Olins, A.L., Gould, T.J., Boyd, L., Sarg, B., and Olins, D.E. (2020). Hyperosmotic stress: in situ chromatin phase separation. Nucleus *11*, 1–18. https://doi.org/10.1080/19491034.2019.1710321.

Pedersen, S.F., Darborg, B.V., Rasmussen, M., Nylandsted, J., and Hoffmann, E.K. (2007). The Na+/H+ exchanger, NHE1, differentially regulates mitogen-activated protein kinase subfamilies after osmotic shrinkage in Ehrlich Lettre Ascites cells. Cell. Physiol. Biochem. *20*, 735–750. https://doi.org/10.1159/000110434.

Pinilla, J., Aledo, J.C., Cwiklinski, E., Hyde, R., Taylor, P.M., and Hundal, H.S. (2011). SNAT2 transceptor signalling via mTOR: a role in cell growth and proliferation? Front. Biosci. *E3*, 1289. https://doi.org/10.2741/332.

Ransom, J.T., and Reeves, J.P. (1983). Accumulation of amino acids within intracellular lysosomes of rat polymorphonuclear leukocytes incubated with amino acid methyl esters. Evidence for the internal acidification of azurophilic granules. J. Biol. Chem. *258*, 9270–9275. https://doi.org/10.1016/s0021-9258(17)44662-x.

Ravi, V., Jain, A., Ahamed, F., Fathma, N., Desingu, P.A., and Sundaresan, N.R. (2018). Systematic evaluation of the adaptability of the non-radioactive SUnSET assay to measure cardiac protein synthesis. Sci. Rep. *8*, 4587. https://doi.org/10.1038/s41598-018-22903-8.

Ray, D., Kazan, H., Cook, K.B., Weirauch, M.T., Najafabadi, H.S., Li, X., Gueroussov, S., Albu, M., Zheng, H., Yang, A., et al. (2013). A compendium of RNA-binding motifs for decoding gene regulation. Nature *499*, 172–177. https://doi.org/10.1038/nature12311.

Ripin, N., and Parker, R. (2022). Are stress granules the RNA analogs of misfolded protein aggregates? RNA *28*, 67–75. https://doi.org/10.1261/rna.079000.121.

Sama, R.R., Ward, C.L., Kaushansky, L.J., Lemay, N., Ishigaki, S., Urano, F., and Bosco, D.A. (2013). FUS/TLS assembles into stress granules and is a pro-survival factor during hyperosmolar stress. J. Cell. Physiol. *228*, 2222–2231. https://doi.org/10.1002/jcp.24395.

Sancak, Y., Bar-Peled, L., Zoncu, R., Markhard, A.L., Nada, S., and Sabatini, D.M. (2010). Ragulator-Rag complex targets mTORC1 to the lysosomal sur-

face and is necessary for its activation by amino acids. Cell *141*, 290–303. https://doi.org/10.1016/j.cell.2010.02.024.

Sanjana, N.E., Shalem, O., and Zhang, F. (2014). Improved vectors and genome-wide libraries for CRISPR screening. Nat Methods *11*, 783–784.

Santra, M., Dill, K.A., and de Graff, A.M.R. (2018). How do chaperones protect a cell's proteins from oxidative damage? Cell Systems *6*, 743–751.e3. https://doi.org/10.1016/j.cels.2018.05.001.

Scheuner, D., Song, B., McEwen, E., Liu, C., Laybutt, R., Gillespie, P., Saunders, T., Bonner-Weir, S., and Kaufman, R.J. (2001). Translational control is required for the unfolded protein response and in vivo glucose homeostasis. Mol. Cell *7*, 1165–1176. https://doi.org/10.1016/s1097-2765(01)00265-9.

Shen, L., and Pelletier, J. (2020). General and target-specific DExD/H RNA helicases in eukaryotic translation initiation. Int. J. Mol. Sci. *21*, 4402. https://doi.org/10.3390/ijms21124402.

Shiraki, K., Kudou, M., Fujiwara, S., Imanaka, T., and Takagi, M. (2002). Biophysical effect of amino acids on the prevention of protein aggregation. J. Biochem. *132*, 591–595. https://doi.org/10.1093/oxfordjournals.jbchem.a003261.

Sidrauski, C., McGeachy, A.M., Ingolia, N.T., and Walter, P. (2015). The small molecule ISRIB reverses the effects of eIF2α phosphorylation on translation and stress granule assembly. Elife *4*, e05033. https://doi.org/10.7554/elife.05033.

Takahara, T., Amemiya, Y., Sugiyama, R., Maki, M., and Shibata, H. (2020). Amino acid-dependent control of mTORC1 signaling: a variety of regulatory modes. J. Biomed. Sci. *27*, 87. https://doi.org/10.1186/s12929-020-00679-2.

Thiemicke, A., and Neuert, G. (2021). Kinetics of osmotic stress regulate a cell fate switch of cell survival. Sci. Adv. *7*, eabe1122. https://doi.org/10.1126/sciadv.abe1122.

Thoreen, C.C., Chantranupong, L., Keys, H.R., Wang, T., Gray, N.S., and Sabatini, D.M. (2012). A unifying model for mTORC1-mediated regulation of mRNA translation. Nature *485*, 109–113. https://doi.org/10.1038/nature11083.

Tsai, J.C., Miller-Vedam, L.E., Anand, A.A., Jaishankar, P., Nguyen, H.C., Renslo, A.R., Frost, A., and Walter, P. (2018). Structure of the nucleotide exchange factor eIF2B reveals mechanism of memory-enhancing molecule. Science *359*, eaaq0939. https://doi.org/10.1126/science.aaq0939.

Uawithya, P., Pisitkun, T., Ruttenberg, B.E., and Knepper, M.A. (2008). Transcriptional profiling of native inner medullary collecting duct cells from rat kidney. Physiol. Genom. *32*, 229–253. https://doi.org/10.1152/physiolgenomics.00201.2007.

Uno, K., Yamada, T., Ishigaki, Y., Imai, J., Hasegawa, Y., Sawada, S., Kaneko, K., Ono, H., Asano, T., Oka, Y., and Katagiri, H. (2015). A hepatic amino acid/mTOR/S6K-dependent signalling pathway modulates systemic lipid metabolism via neuronal signals. Nat. Commun. *6*, 7940. https://doi.org/10.1038/ncomms8940.

Valentin-Vega, Y.A., Wang, Y.D., Parker, M., Patmore, D.M., Kanagaraj, A., Moore, J., Rusch, M., Finkelstein, D., Ellison, D.W., Gilbertson, R.J., et al. (2016). Cancer-associated DDX3X mutations drive stress granule assembly and impair global translation. Sci. Rep. *6*, 25996. https://doi.org/10.1038/srep25996.

van Ommen, B., Hendriks, W., Bessems, J.G., Geesink, G., Müller, F., and van Bladeren, P.J. (1989). The relation between the oxidative biotransformation of hexachlorobenzene and its porphyrinogenic activity. Toxicol. Appl. Pharmacol. *100*, 517–528. https://doi.org/10.1016/0041-008x(89)90299-8.

Wang, L., Wang, S., and Li, W. (2012). RSeQC: quality control of RNA-seq experiments. Bioinformatics *28*, 2184–2185. https://doi.org/10.1093/bioinformatics/bts356.

Watanabe, K., Morishita, K., Zhou, X., Shiizaki, S., Uchiyama, Y., Koike, M., Naguro, I., and Ichijo, H. (2021). Cells recognize osmotic stress through liquid-liquid phase separation lubricated with poly(ADP-ribose). Nat. Commun. *12*, 1353. https://doi.org/10.1038/s41467-021-21614-5.

Yancey, P.H., Clark, M.E., Hand, S.C., Bowlus, R.D., and Somero, G.N. (1982). Living with water stress: evolution of osmolyte systems. Science *217*, 1214–1222. https://doi.org/10.1126/science.7112124.

Yasuda, S., Tsuchiya, H., Kaiho, A., Guo, Q., Ikeuchi, K., Endo, A., Arai, N., Ohtake, F., Murata, S., Inada, T., et al. (2020). Stress- and ubiquitylation-dependent phase separation of the proteasome. Nature *578*, 296–300. https://doi.org/10.1038/s41586-020-1982-9.

Zyryanova, A.F., Weis, F., Faille, A., Alard, A.A., Crespillo-Casado, A., Sekine, Y., Harding, H.P., Allen, F., Parts, L., Fromont, C., et al. (2018). Binding of ISRIB reveals a regulatory site in the nucleotide exchange factor eIF2B. Science *359*, 1533–1536. https://doi.org/10.1126/science.aar5129.

CellPress
OPEN ACCESS

STAR★METHODS

KEY RESOURCES TABLE

REAGENT or RESOURCE	SOURCE	IDENTIFIER
Antibodies		
Rabbit polyclonal anti-ATF4	Proteintech	Cat# 10835-1-AP, RRID: AB_2058600
Mouse monoclonal anti-eIF2α	Santa Cruz Biotechnology	Cat# sc-133227; RRID: AB_2096505
Rabbit monoclonal anti-eIF2α-phospho (Ser51)	Abcam	Cat# ab32157; RRID: AB_732117
Rabbit polyclonal anti-GADD34	Proteintech	Cat# 10449-1-AP; RRID: AB_2168724
Rabbit polyclonal anti-SNAT2	MBL International	Cat# BMP081; RRID: AB_10597880
Rabbit anti-FUS	Sigma-Aldrich	Cat# HPA008784; RRID: AB_1849181
Mouse monoclonal anti-DDX3X	Santa Cruz Biotechnology	Cat# sc-365768; RRID: AB_10844621
Rabbit anti-DDX3X	Bethyl	Cat# A300-474A; RRID: AB_451009
Mouse monoclonal anti-G3BP1	Santa Cruz Biotechnology	Cat# sc-365338; RRID: AB_10846950
Mouse monoclonal anti- Puromycin	Millipore	Cat# MABE342; RRID: AB_2737590
Rabbit polyclonal anti-S6K	Cell Signaling Technology	Cat# 9202; RRID: AB_331676
Rabbit polyclonal anti-S6K-phospho (Thr389)	Cell Signaling Technology	Cat# 9205; RRID: AB_330944
Rabbit polyclonal anti-S6	Cell Signaling Technology	Cat# 2895; RRID: AB_2089254
Rabbit monoclonal anti-S6-phospho (Ser235/236)	Cell Signaling Technology	Cat# 2211; RRID: AB_331679
Rabbit monoclonal anti-4E-BP1	Cell Signaling Technology	Cat# 9644; RRID: AB_2097841
Rabbit polyclonal anti-HSPB8	Proteintech	Cat# 15287-1-AP; RRID: AB_2248640
Rabbit polyclonal anti-HSP27	Enzo Life Sciences	Cat# ADI-SPA-803-D; RRID: AB_2039220
Rabbit monoclonal anti-HSP27-phospho (Ser82)	Cell Signaling Technology	Cat# 9709; RRID: AB_11217429
Goat anti-Mouse IgG (H+L) Highly Cross-Adsorbed Secondary Antibody, Alexa Fluor Plus 594	Thermo Fisher Scientific	Cat# A32742; RRID: AB_2762825
Goat anti-Rabbit IgG (H + L) Highly Cross-Adsorbed Secondary Antibody, Alexa Fluor Plus 594	Thermo Fisher Scientific	Cat# A32740; RRID: AB_2762824
Goat anti-Rabbit IgG (H + L) Highly Cross-Adsorbed Secondary Antibody, Alexa Fluor Plus 488	Thermo Fisher Scientific	Cat# A32731; RRID: AB_2633280
Goat anti-Mouse IgG (H + L) Highly Cross-Adsorbed Secondary Antibody, Alexa Fluor Plus 488	Thermo Fisher Scientific	Cat# A32723; RRID: AB_2633275
Goat anti-Mouse IgG (H + L) Cross-Adsorbed Secondary Antibody, HRP	Thermo Fisher Scientific	Cat# G-21040; RRID: AB_2536527
Goat anti-Rabbit IgG (H + L) Cross-Adsorbed Secondary Antibody, HRP	Thermo Fisher Scientific	Cat# G-21234; RRID: AB_2536530
Chemicals, peptides, and recombinant proteins		
Penicillin-Streptomycin-Glutamine (100×)	Thermo Fisher Scientific	Cat# 10378016
Gibco™ Fetal Bovine Serum, qualified	Thermo Fisher Scientific	Cat# 26140079
cOmplete™, Mini, EDTA-free Protease Inhibitor Cocktail	Roche	Cat# 04693159001
PhosSTOP	Roche	Cat# 04906837001
ISRIB	Millipore Sigma	Cat# SML0843

(Continued on next page)

Continued

REAGENT or RESOURCE	SOURCE	IDENTIFIER
GCN2iB	MedChemExpress	Cat# HY-112654
Sal003	Tocris	Cat# 3657
torin 1	Tocris	Cat# 4247
α-(Methylamino)isobutyric acid (MeAIB)	Millipore Sigma	Cat# M2383
EasyTag™ EXPRESS35S Protein Labeling Mix	PerkinElmer	Cat# NEG072007MC
L-[3,4,5-^{3}H(N)]-Leucine	PerkinElmer	Cat# NET460001MC
L-[2,3,4,5-^{3}H]-Proline	PerkinElmer	Cat# NET483001MC
L-[3,4-^{3}H(N)]-Glutamine	PerkinElmer	Cat# NET551001MC
Guanosine 5′-Diphosphate, Trisodium Salt, [8,5′-^{3}H]	PerkinElmer	Cat# NET96600
α-[1–^{14}C]-Methylaminoisobutyric Acid	PerkinElmer	Cat# NEC671250UC
L-Leu	Millipore Sigma	Cat# L8000
L-Gln	Millipore Sigma	Cat# G3126
L-Thr	Millipore Sigma	Cat# T8625
L-Pro	Millipore Sigma	Cat# P0380
L-Leucyl-L-Leucine methyl ester (LLME)	Cayman	Cat# 16008
Puromycin dihydrochloride	Thermo Fisher Scientific	Cat# A1113803
X-tremeGENE™ 9 DNA Transfection Reagent	Roche	Cat# 6365787001
Krebs-Ringer Bicarbonate Buffer	Millipore Sigma	Cat# K4002
TRIzol Reagent	Thermo Fisher Scientific	Cat# 15596018
TRIzol Reagent LS	Thermo Fisher Scientific	Cat# 10296028
Cycloheximide	Millipore Sigma	Cat# C7698
Trichloroacetic acid (TCA)	Millipore Sigma	Cat# T0699
IGEPAL	Millipore Sigma	Cat# I8896
RNase Inhibitor, Murine	NEB	Cat# M0314L
Ambion™ RNase I, cloned, 100 U/μL	Thermo Fisher Scientific	Cat# AM2295
SYBR™ Gold Nucleic Acid Gel Stain	Thermo Fisher Scientific	Cat# S11494
Novex™ TBE-Urea Gels, 15%, 10 well	Thermo Fisher Scientific	Cat# EC6885BOX
Novex™ TBE-Urea Gels, 10%, 10 well	Thermo Fisher Scientific	Cat# EC6875BOX
Novex™ TBE Gels, 8%, 10 well	Thermo Fisher Scientific	Cat# EC6215BOX
GlycoBlue™ Coprecipitant	Thermo Fisher Scientific	Cat# AM9515
Corning® Costar® Spin-X® centrifuge tube filters	Millipore Sigma	Cat# CLS8160
Carbonyl Cyanide Chlorophenylhydrazone (CCCP)	Millipore Sigma	Cat# C2759
T4 Polynucleotide Kinase	NEB	Cat# M0201S
T4 RNA ligase truncated KQ	NEB	Cat# M0373
5′ DNA Adenylation Kit	NEB	Cat# E2610S
NEBNext® Multiplex Oligos for Illumina®	NEB	Cat# E7335S
NEBNext® Ultra™ II Q5® Master Mix	NEB	Cat# M0544S
CircLigase™ ssDNA Ligase	Lucigen	Cat# CL4111K
SuperScript™ III Reverse Transcriptase	Thermo Fisher Scientific	Cat# 18080044
MyOne streptavidin C1 DynaBeads	Thermo Fisher	Cat# 65001
Glass microfiber filters (Whatman)	GE Healthcare Life Sciences	Cat# 1822-025
Deposited data		
NGS data	GEO Series accession number	GEO: GSE200097
Experimental models: Cell lines		
10.014 pRSV-T human corneal epithelium	ATCC	Cat# CRL-11515; RRID:CVCL_6341
S51A Mouse Embrionic Fibroblasts	https://doi.org/10.1016/s1097-2765(0100265-9)	N/A

Continued

REAGENT or RESOURCE	SOURCE	IDENTIFIER
Oligonucleotides		
Oligos for Ribosome footprinting	Integrated DNA Technologies	See Table S2
Oligos for sgRNA subcloning	Integrated DNA Technologies	See Table S2
Oligos for qPCR	Integrated DNA Technologies	see Table S2
Recombinant DNA		
lentiCRISPR v2	Addgene	Plasmid #52961
MISSION shRNA targeting SNAT2 #1	MilliporeSigma	Cat# TRCN0000020239
MISSION shRNA targeting SNAT2 #2	MilliporeSigma	Cat# TRCN0000020240
MISSION pLKO.1-puro Empty Vector Control Plasmid DNA	MilliporeSigma	Cat# SHC001
psPAX2	Addgene	Cat# 12260
pMD2.G	Addgene	Cat# 12259
lentiCRISPR V2 targeting mouse SNAT2	this work	N/A
Software and algorithms		
Origin	Origin Labs	https://www.originlab.com/demodownload.aspx
Cutadapt (ver. 1.18)	https://cutadapt.readthedocs.io/en/stable/	https://doi.org/10.14806/ej.17.1.200
BBmap (ver. 36.59)	https://www.osti.gov/biblio/1241166	N/A
hisat2 (ver. 2.1.0)	http://daehwankimlab.github.io/hisat2/	N/A
HTseq (ver. 0.11.4)	http://www-huber.embl.de/HTSeq	https://doi.org/10.1093/bioinformatics/btu638
riboWaltz (ver 1.1.0)	https://github.com/LabTranslationalArchitectomics/riboWaltz	(Lauria et al., 2018)
RUST (ver. 1.2) (O'Connor et al., 2016).	https://github.com/LabTranslationalArchitectomics/riboWaltz	O'Connor et al. (2016)
RSeQC (ver. 2.6.6)	http://rseqc.sourceforge.net/	Wang et al. (2012)
anota2seq (ver. 1.4.2)	https://bioconductor.statistik.tu-dortmund.de/packages/3.8/bioc/html/anota2seq.html	Oertlin et al. (2019)
ClueGO (ver. 2.5.7)	https://apps.cytoscape.org/apps/cluego	Bindea et al. (2009)
Dreme	http://meme.nbcr.net	https://doi.org/10.1093/bioinformatics/btr261
Tomtom	https://web.mit.edu/meme_v4.11.4/share/doc/overview.html	https://doi.org/10.1186/gb-2007-8-2-r24

RESOURCE AVAILABILITY

Lead contact
Further information and requests for resources and reagents should be directed to and will be fulfilled by the lead contact, Maria Hatzoglou (mxh8@case.edu).

Materials availability
Plasmid generated in this study will be made available on request. Maria Hatzoglou (mxh8@case.edu)

Data and code availability

The data of ribosome profiling and RNA-seq obtained in this publication have been deposited in NCBI's Gene Expression Omnibus and are accessible through GEO Series accession number GEO: GSE200097.

This paper does not report original code.

Any additional information required to reanalyze the data reported in this paper is available from the lead contact, Maria Hatzoglou (mxh8@case.edu) upon request.

EXPERIMENTAL MODEL AND SUBJECT DETAILS

Cell lines, cell culture treatments and chemicals

Immortalized human corneal epithelial cell line 10.014 pRSV-T (ATCC, CRL-11515) were grown in Keratinocyte-SFM (Thermo Fisher Scientific, 17005–042) supplemented with 5 ng/mL human recombinant Epidermal Growth Factor (rEGF), 0.05 mg/mL Bovine Pituitary Extract (BPE), 0.005 mg/mL bovine insulin (Sigma-Aldrich, I1882) and 500 ng/mL Hydrocortisone (Sigma-Aldrich, H0135). Cell culture dishes were precoated with Dulbecco's phosphate-buffered saline (DPBS) (Thermo Fisher Scientific, 14040182) containing 0.01 mg/mL Fibronectin (Sigma-Aldrich, F0895), 0.03 mg/mL Bovine Collagen Type I (Thermo Fisher Scientific, 50-360-230) and 0.01 mg/mL Bovine Serum Albumin (BSA)(Sigma-Aldrich, A8022). eIF2$\alpha^{S51A/S51A}$ MEFs (Scheuner et al., 2001) were grown in high glucose Dulbecco's modified Eagle's medium (DMEM) (Thermo Fisher Scientific, 11960044) supplemented with 10% fetal bovine serum (Thermo Fisher Scientific, 26140079), 1× Penicillin-Streptomycin-Glutamine (Thermo Fisher Scientific, 10378016). Cells were maintained in a humidified atmosphere of 5% CO_2 at 37°C. Hyperosmotic stress was induced with NaCl (Sigma-Aldrich, S9888). Other chemicals used in this study include Cycloheximide (CHX) (100 μg/mL) (Sigma-Aldrich C7698), Sephin1 (Apexbio, A8708), Sal 003 (1 μM) (Tocris Bioscience, 3657), torin 1 (Tocris Bioscience, 4247), α-(Methylamino)isobutyric acid (MeAIB) (Sigma-Aldrich, M2383), L-Leucyl-L-Leucine methyl ester (LLME) (Cayman Chemical, 16008), Puromycin (Thermo Fisher Scientific, A1113803), GCN2iB (Medchemexpress, HY-112654), ISRIB (Tocris, 5284).

METHOD DETAILS

Protein extraction and western blot analysis

Cells were washed twice with ice-cold DPBS and scraped into lysis buffer (50 mM Tris-HCl at pH 7.5, 150 mM NaCl, 2 mM EDTA, 1% IGEPAL, 0.1% SDS, and 0.5% sodium deoxycholate) supplemented with EDTA-free protease inhibitor (Roche, 04693159001) and PhosSTOP phosphatase inhibitor (Roche, 04906837001) (1 tablet of each per 10 mL), and sonicated briefly 10 times (2 RMS). After centrifugation (12000 × g, 10 min, 4°C), proteins were quantified using the DC Protein Assay Kit (Bio-Rad, 500–0113 and 500–0114). Equal amounts of protein (10–20 μg) were analyzed by Western blotting. Densitometric analysis of selected Western blots was performed using Image J. Primary antibodies used in this study are listed in key resources table.

Gene knockdown experiments

Plasmid expressing shRNA against human SNAT2 (Sigma-Aldrich, TRCN0000020239 and TRCN0000020241) and MISSION® pLKO.1-puro Non-Target shRNA Control Plasmid DNA (Sigma-Aldrich, SHC016)) were purchased from Sigma-Aldrich. HEK 293T cells (150 mm dishes, 50% confluency) (ATCC, CRL-3216) were transfected with 12.5 μg shRNA expressing vector: 8 μg viral packaging plasmid (psPAX2 (Addgene,12260)): 4.5 μg viral envelope plasmid (pMD2.G (Addgene,12259)) ratio with X-tremeGENE™ 9 DNA Transfection Reagent (Roche, 6365779001) according to the manufacturer's instructions. After transfection, cells were maintained in corneal growth media which was collected after 24, 48 and 72 h and filtered through 0.45 μM filter. The filtrate was diluted with the corneal growth media (4:1 ratio) supplemented with Hexadimethrine bromide (Sigma-Aldrich, H9268) at 10μg/mL and added to the corneal cells for 12 h followed by 12 h in the growth media without viral particles. The procedure was repeated once more and cells were allowed to recover one day in the growth media. After this, cells were subcultured and grown in media containing 1 μg/mL puromycin. After 3–4 days of the selection with puromycin cells were used for experiments. Knockdown efficiency was verified by Western blot analysis.

Generation of SLC38A2 knock-out cell line using CRISPR-CAS9

sgRNAs targeting the first exon of mouse SLC38A2 were identified using http://crispr.mit.edu/online tool and subcloned into BsmBI cut lentiCRISPR v2 plasmid (Addgene, 52961) (Sanjana et al., 2014) using a set of primers to anneal (CAC CGT TCA ACA TCT CCC CGG ATG; AAA CCA TCC GGG GAG ATG TTG AAC). Insert position was verified by sequencing. Propagation of lentiviral particles expressing lentiCRISPR sgSLC38A2 was performed in HEK293T cells. S51A MEFs were infected with the lentivirus and 24 h later, cells were selected with puromycin (2.5 μg/mL) for 3 days. The deletion was verified by western blotting.

Amino acid uptake assays

For Amino acid uptake studies: cells were grown in 24-well plates, and for SNAT2 activity the uptake of 100 μM meAIB with 3μCi/mL of α-[1–^{14}C]-Methylaminoisobutyric Acid (PerkinElmer, NEC671250UC) or L-Pro with 3 μCi/mL of L-[2,3,4,5-^{3}H]-Proline (PerkinElmer,

NET483250UC) was measured in Earle's 1× Balanced Salt Solution (EBSS) (Thermo Fisher Scientific, SH3002902) in the presence of Na⁺ ions for 3 min at 37°C. LAT1 activity uptake was tested with 10 L-Leu with 3 μCi/ml μM L-[3,4,5-³H(N)]-Leucine (PerkinElmer, NET460250UC) in modified EBSS with Na⁺ replaced with choline. Glutamine uptake was tested with 50 μM L-Gln with 3 μCi/ml L-[3,4-³H(N)]-Glutamine (PerkinElmer, NET551250UC) in EBSS. For competitive inhibition amino acids or MeAIB were added to transport reaction at 5 mM concentration. After assay, cells were washed twice with ice-cold DPBS to remove the labeled compound, and the intracellular amino acid pool was extracted with ethanol. Radioactivity was measured using a scintillation counter and normalized to protein content. Experiments data are presented as average (n = 4–6), error bars represent SD.

Measurement of protein synthesis rates via puromycin incorporation and metabolic labeling with [³⁵S]-Met/Cys

Protein synthesis rates were measured using two different methods: 1. 1 μM Puromycin was added to the cell culture media for the last 20 min of treatment and cells were lysed in RIPA buffer and equal amount of proteins were used for the Western blot analysis via anti-Puromycin mouse monoclonal antibodies as described (Ravi et al., 2018). 2. Metabolic labeling with [³⁵S]-Met/Cys:

Cells on 24-well dishes were treated with appropriate stress conditions, followed by incubation with [³⁵S]-Met/Cys (30 μCi/mL EXPRE³⁵S³⁵S Protein Labeling Mix, PerkinElmer, NEG072007MC) for an additional 30 min. After quickly washing with ice-cold PBS twice, cells were incubated with 5% trichloroacetic acid (TCA)/1 mM cold methionine for 10 min on ice (repeated three times) and lysed in 200 μL of 1 N NaOH/0.5% sodium deoxycholate for 1 h. Incorporation of radioactive amino acids was determined by liquid scintillation counting and normalized to the cellular protein content (quantified with DC Protein Assay (Bio-Rad)).

Measuring in vitro guanine nucleotide exchange factor (GEF) activity of eIF2B

GEF activity of the cellular extracts was assayed as previously described (Kimball et al., 1989; Guan et al., 2017). Briefly, after washing twice with ice-cold PBS, cells were lysed in the homogenization buffer (45 mM HEPES-KOH at pH 7.4, 0.375 mM MgOAc, 75 μM EDTA, 95 mM KOAc, 10% glycerol, 1 mM DTT, 2.5 mg/mL digitonin, protease and phosphatase inhibitors (Roche Applied Science; 1 tablet per 10 mL)). Cell lysates were incubated on ice for 15 min, vortexed occasionally, passed six times through a 26-gauge needle, and centrifuged at 13,000 rpm for 15 min at 4°C. After determining protein concentration using the DC Protein Assay (Bio-Rad), 100 μg was used for the assay. eIF2 (purified from rabbit reticulocyte lysate) was incubated with [³H]-GDP for 10 min at 30°C in buffer (62.5 mM MOPS at pH 7.4, 125 mM KCl, 1.25 mM DTT, 0.25 mg/mL bovine serum albumin (BSA)). The complex was stabilized by the addition of 2.5 mM MgOAc and incubated with nonradioactive GDP (0.1 mg/mL)-supplemented lysate at 30°C. At 0, 2, 4, and 6 min, aliquots of the mixture were removed and filtered through nitrocellulose filters. The amount of eIF2α-[³H]-GDP complex bound to the nitrocellulose filters was assessed by liquid scintillation counting. The eIF2B activity was calculated as the rate of exchange of [³H]-GDP for nonradioactive GDP.

Amino acid analysis

Amino acid levels were determined after extraction with 5% acetic acid in ethanol. Samples were lyophilized and resuspended in 100 mM borate buffer (pH 9.5) and analyzed after derivatization with a UPLC amino acid analysis instrument (Waters) at Golden LEAF Biomanufacturing Training and Education Center, North Carolina State University or UF-Amino station (Shimadzu) at EcoTech Complex, MC Sklodowska University.

Ribosome footprinting analysis

Three 150 mm dishes of pRSV-T cells (80% confluency) were treated with hypertonic stress. To avoid potential artifacts of pre-treating live cells with cycloheximide (Gerashchenko and Gladyshev, 2014), cycloheximide was added to the lysis buffer only after cells were harvested as previously described (Calviello et al., 2016; Darnell et al., 2018; Gerashchenko and Gladyshev, 2014; Mao et al., 2019). After washing three times with ice-cold PBS, cells were scraped in 1 mL lysis buffer (10 mM HEPES pH 7.4, 5 mM MgCl₂, 100 mM KCl, 1% Triton X-,100 μg/mL cycloheximide, 2 mM DTT, RNase inhibitor (1:100 dilution, NEB, M0314L), protease inhibitor (1 tablet per 10 mL, Roche, 04693159001). The lysate was passed four times through a 26G needle and centrifuged at 1300 × g for 10 min. Lysate (OD A260 = 10) was loaded on a linear 10%–50% sucrose gradient (gradient buffer is the same as the lysis buffer, lacking only Triton X- and Protease and RNase inhibitors) and centrifuged at 4°C at 31,000 rpm for 2.5 h using an SW 32 Ti rotor (Beckman Coulter, 369694). The gradients were fractionated using a Teledyne ISCO Density Gradient Fractionation System and 12 fractions were collected. The fractions from (including) the 80S peak to the bottom of the gradient were combined. 300 μL of the combined fractions was digested with 5 μL RNase I (Thermo Fisher Scientific, AM2295) for 1 h at 4°C (with slow rotation on a nutator). Immediately, Trizol LS (Thermo Fisher Scientific, 10296028) was added, and RNA isolated according to the manufacturer's instructions. 10 μg of total RNA isolated from the combined fractions was resolved by 15% TBE-Urea gel (Thermo Fisher Scientific, EC6885BOX) and visualized with SYBR™ Gold Nucleic Acid Gel Stain (Thermo Fisher Scientific, S11494); the 28–30 nt region was excised from the gel. The RNA was eluted in 400 μL RNA elution buffer (EB) at 4°C overnight (RNA EB: 0.3M sodium acetate (NaOAc, pH 5.5), 1 mM EDTA, 0.4 U/μL RNase inhibitor). Gel debris was removed using Corning Costar Spin-X centrifuge tube filters (Sigma-Aldrich, CLS8160). RNA was precipitated with 4 μL GlycoBlue Coprecipitant (Thermo Fisher Scientific, AM9515), 40 μL sodium acetate, and 1 mL ethanol overnight at −80°C. Recovered footprints were dephosphorylated in a 15 μL reaction mixture (1 μL T4 PNK (NEB, M0201S), 10× T4 PNK buffer, 0.4 U/μL RNase inhibitor) at 37°C for 1 h followed by heat inactivation at 65°C for 10 min. Dephosphorylated RNA was precipitated as described above and recovered in 4 μL of water. Pre-adenylated DNA linker (DNA oligo purchase from IDT was adenylated using 5′ DNA Adenylation Kit (NEB, E2610S))

was ligated to the 3′-end of RNA in a 20 μL reaction (25% PEG8000, 1× T4 RNA ligase buffer, 1 mM DTT, 0.4 U/μL murine RNase inhibitor, 300 U T4 RNA ligase truncated KQ (NEB, M0373S), 1 μM pre-adenylated DNA linker) for 6 h at 25°C followed by overnight ethanol precipitation as described above. Ligated footprints were resolved by 10% TBE-Urea Gel (Thermo Fisher Scientific, EC6875BOX), purified, eluted in the RNA EB at 4°C overnight, precipitated at −80°C as described above and resuspended in 10.5 μL water. 1 μL of 2.5 μM RT primer was added and heated at 65°C for 5 min, cooled on ice and incubated in 20 μL RT mix (300 U Superscript III (Thermo Fisher Scientific, 18080044), 1× RT buffer, 500 μM dNTPs, 5 mM DTT) for 30 min at 55°C, then heat inactivated at 70°C for 15 min. RT product was precipitated with ethanol as described above, resuspended in 10 μL water and resolved by 10% TBE-Urea gel. cDNA was isolated and eluted overnight in DNA elution buffer (DNA EB: 0.3 M NaCl, 1 mM EDTA), precipitated overnight, recovered and used for the 20 μL circularization reaction (100 U CircLigase ssDNA Ligase (Lucigen, CL4111K), 50 mM ATP, 2.5 mM MnCl2, 1× Circligase buffer) at 60°C for 2 h. rRNA depletion was performed according to Ingolia et al., (2012). Circularized, rRNA-depleted cDNA was used in the PCR using NEBNext Ultra II Q5 Master Mix (NEB, M0544S) and NEBNext Multiplex Oligos for Illumina (NEB, E7335S). Half of the cDNA was used to determine the optimal PCR cycle number. The PCR products were resolved by 8% TBE gel (Thermo Fisher Scientific, EC6215BOX). The other half of the cDNA was amplified by the determined PCR cycle, resolved by 8% TBE gel, and PCR products were cut, eluted in DNA EB, precipitated as described above, and recovered in 15 μL water. The quality and quantity of libraries were confirmed using DNA High Sensitivity Bioanalyzer (Agilent). Equal amounts of libraries were mixed and sequenced using SE75, NextSeq 500 (Illumina) sequencing platform.

Cytoplasmic RNA levels
RNA was isolated from the cytoplasmic lysate (input that was loaded on the sucrose gradients for the abovementioned ribosome footprinting analysis) using Trizol LS according to the manufacturer's instructions, except that precipitation with isopropanol was conducted overnight at −80°C. 1 μg RNA was depleted from rRNA using NEBNext rRNA Depletion Kit (Human/Mouse/Rat) (NEB, E6310L) and was used to make libraries with NEBNext Ultra™ II Directional RNA Library Prep (NEB, E7765S) according to the manufacturer's instructions. The quality and quantity of libraries were confirmed using DNA High Sensitivity Bioanalyzer (Agilent) and sequenced using PE150, NovaSeq sequencing platform.

Ribosomal footprinting data analysis
Cutadapt (ver 1.18) (https://doi.org/10.14806/ej.17.1.200) (-q 10 -e 0.15 -O 1 -n 4 -m 20) was used to trim reads for adapter sequence: 'CTGTAGGCACCATCAATAGATCGGAAGAGCACACG TCTGAACTCCAGTCAC' and first 6 nucleotides of each read (-u 6 -u −4 -m 20). Reads matching ribosomal RNA sequences obtained from RefSeq database were removed using BBmap (ver. 36.59) (https://www.osti.gov/biblio/1241166). Resulting reads were aligned to RefSeq hg38 genome using hisat2 (ver. 2.1.0) (Kim et al., 2015). In order to extract the genuine ribosome footprints, reads with a length (22–29 inclusive) were used for further analysis. Subsequently the uniquely mapped reads were summarized using HTseq (ver. 0.11.4) (Anders et al., 2015). Finally, QC analysis was conducted with help of riboWaltz (ver 1.1.0) (Lauria et al., 2018) and RUST (ver. 1.2) (O'Connor et al., 2016).

RNA-seq data analysis
Reads were trimmed for Nextera adapters using BBmap (ver. 36.59) (https://www.osti.gov/servlets/purl/1241166) (k = 13 ktrim = n useshortkmers = t mink = 5 qtrim = t trimq = 10 minlength = 25) and subsequently aligned to RefSeq hg38 genome using hisat2 (ver. 2.1.0) (Kim et al., 2015) and summarized using HTseq (ver. 0.11.4) (Anders et al., 2015). Finally, the output files were verified with RSeQC (ver. 2.6.6) (Wang et al., 2012).

Analysis of differential translation with anota2seq
Genes with 0 counts in at least one sample were discarded resulting in 10178 unique genes. The remaining data were TMM-log2 normalized and analyzed for changes in using the anota2seq algorithm (ver. 1.4.2) (Oertlin et al., 2019), with "replicate" included in the model to account for batch effects (using the batchVec argument in anota2seq) (minSlopeTranslation = −1, maxSlopeTranslation = 2, minSlopeBuffering = −2, maxSlopeBuffering = 1, deltaPT = log2(1.5), deltaP = log2(1.5), deltaTP = log2(1.5), deltaT = log2(1.5), significance threshold maxRvmPAdj = 0.15 [i.e. FDR <0.15]. To classify genes into translation, buffering or mRNA abundance gene expression modes, the anota2seqRegModes function within anota2seq was used.

Motif discovery
The software Dreme (Bailey, 2011) from the MEME suite (Bailey et al., 2009) was used to identify over-represented motifs (E value <0.001). Subsequently, Tomtom (Gupta et al., 2007) was applied to match (with q-value 0.01) identified motifs to RBPs in the Ray2013 database (Ray et al., 2013). Then, the presence of the motif across transcripts was then determined.

mRNA's general features analysis
GC content and length of mRNAs modulated during the early (1 h hyperosmotic stress vs control) or adaptive (6 h vs 1 h of hyperosmotic stress) phases were calculated based on RefSeq hg38 sequences, presented as violin plots and compared to all other expressed genes. Representative isoforms were selected randomly for multitranscript genes. p-values from Wilcoxon tests comparing all transcript subsets to the background (grey) are indicated.

Polysome profile and qPCR analysis

The lysate preparation and centrifugation conditions were identical to those described in the ribosome footprinting analysis. 12 fractions (each 1.2 mL) were collected, and RNA from each fraction was isolated using TRIzol LS reagent. An equal volume of RNA from each fraction was used for cDNA synthesis using the SuperScript™ III First-Strand Synthesis SuperMix for qRT-PCR (Thermo Fisher Scientific, 11752250). The relative quantity of specific mRNAs was measured by reverse transcriptase (RT)-quantitative polymerase chain reaction (qPCR) using VeriQuest SYBR Green qPCR Master Mix (Thermo Fisher Scientific, 756001000RXN) with the StepOnePlus Real-Time PCR System (Thermo Fisher Scientific, 4376599). For the list of primers see Table S1.

Microscopy

Human corneal cells were cultured on coverslips. Following treatment, cells were washed twice with cold DPBS, fixed with 4% paraformaldehyde (Thermo Fisher Scientific, J19943-K2) for 15 min at RT, washed twice with cold DPBS, and permeabilized with 0.2% Triton X-100 (MilliporeSigma, ×100) for 10 min at RT. After blocking (blocking buffer: 0.2% Triton X-100, 10% FBS in DPBS) for 1 h at RT, cells were incubated with the primary antibody in the blocking buffer at 4°C for 16 h. Cells were washed with 0.2% Triton X-100 and incubated with fluorescent-dye conjugated secondary antibody for 2 h at RT in the dark. Cells were washed twice 0.2% Triton X-100 and DNA was labeled with Hoechst 33324 (Thermo Fisher Scientific, 62249) for 5 min. Images were acquired with Leica SP8 and Olympus FV1000 confocal microscope. Raw images were acquired with 16-bit depth. 63× objective lens with 1.5× magnification was used. In this condition, the axial resolution of all raw images was 512 × 512 pixel. Z-stacks of 5 planes (2 μM deep) were reconstructed into a single image with maximum intensity projection by ImageJ software. The quantification of the fluorescence intensity was done using ImageJ software. In brief, for FUS protein: the region of interest, for example, cytoplasm region, was assigned by Polygon Selection and the average fluorescence intensity was measured. The average intensity of five random blank regions in the same image was calculated as background. The recorded intensity was calculated by Polygon Selected intensity substrate with the background. All cell signal in an image was measured and calculated. For number DDX3X of cytoplasmic inclusions quantification was performed by using AggreCount Add-in in ImageJ software (Klickstein et al., 2020). In brief, the region of interest, for example, the cytoplasm region, was assigned. An average intensity of five random blank regions (without visible aggregates) in the same image was calculated as the threshold. The number of aggregates each cell was measured for a statistics analysis.

DDX3X purification

DDX3X was expressed from a pET-SUMO plasmid in BL21 (DE3) E. coli for 4 h with 0.5 mM Isopropyl ß-D-1-thiogalactopyranoside at 37°C. Expression was induced when culture reached OD600–0.6. Bacteria were lysed on ice by sonication in 1× lysis buffer (1× buffer Y (50 mM NaH2PO4 pH 6.0, 300 mM NaCl, 30% glycerol) supplemented with 0.5% IGEPAL, 5 mM imidazole, 1 mM PMSF, and EDTA-free protease inhibitor. Lysates were initially purified on Ni-NTA-agarose using 4–5 column volume washes with wash buffer 1 (1× buffer Y supplemented with 1M NaCl, 5 mM imidazole, 1% IGEPAL, 0.4 mM PMSF), wash buffer 2 (1× buffer Y supplemented with 30 mM imidazole, 1% IGEPAL, 0.4 mM PMSF), and wash buffer 3 (1× buffer Y supplemented with 60 mM imidazole, 1% IGEPAL, 0.4 mM PMSF). DDX3X was then eluted with 1× buffer Y with 350 mM imidazole, 1% IGEPAL, 0.4 mM PMSF. DDX3X-containing fractions were pooled and diluted three-fold with 1× buffer Z (100 mM Tris-Cl pH 8.0, 1 mM EDTA, 50% glycerol, 0.1% Triton X-100, 2 mM DTT) and incubated with SUMO protease overnight at 4°C to remove the His-SUMO tag. Cleaved protein was then bound to phosphocellulose resin and washed with 10 column volumes of wash buffer 1 (1× buffer Z with 50 mM NaCl) and wash buffer 2 (1× buffer Z with 100 mM NaCl) to remove excess SUMO protease. DDX3X was then eluted with 1× buffer Z with 200 mM NaCl. Purified protein was pooled, concentrated using a 10 kDa centrifugal filter unit (Millipore, UFC8010), and snap frozen.

In vitro phase separation of DDX3X

2 μM DDX3X was incubated with 100 nM Alexa Fluor 647-labeled DDX3X and increasing concentrations of proline for 2 h at 25°C in helicase reaction buffer (40 mM Tris pH 8; 0.5mM MgCl₂; 0.01% IGEPAL CA-630; 2mM DTT; 53.33 mM NaCl; 13.33% glycerol). Following incubation, 10 μL of reaction was plated on a slide, topped with a coverslip, and imaged on a Leica DM6000 upright microscope at 20×. 20 images (both fluorescence and DIC) were obtained for each condition. Fluorescent images were quantified using the nucleus counter feature of ImageJ with the following parameters: smallest particle size 1 μm, largest particle size 10,000 μm, Otsu thresholding, no smoothing, with background subtraction and watershed filter applied.

QUANTIFICATION AND STATISTICAL ANALYSIS

At least three independent experiments or biological replicates were used to generate all quantitative data and presented as mean ± SEM. All statistics is included in the Figure Legends. For ribosome footprinting and RNA-seq, four biological replicates were analyzed. For Figures 1, 2, 5, 6, and S1–S3, two-way ANOVA, was used to indicated a significant difference between groups, and post hoc Tukey's range test, indicated a significant difference between a pairwise comparison (Origin software). A p value of less than 0.05 was considered statistically significant (*$p < 0.05$).